Background uptake of monoclonal antibodies in the brain

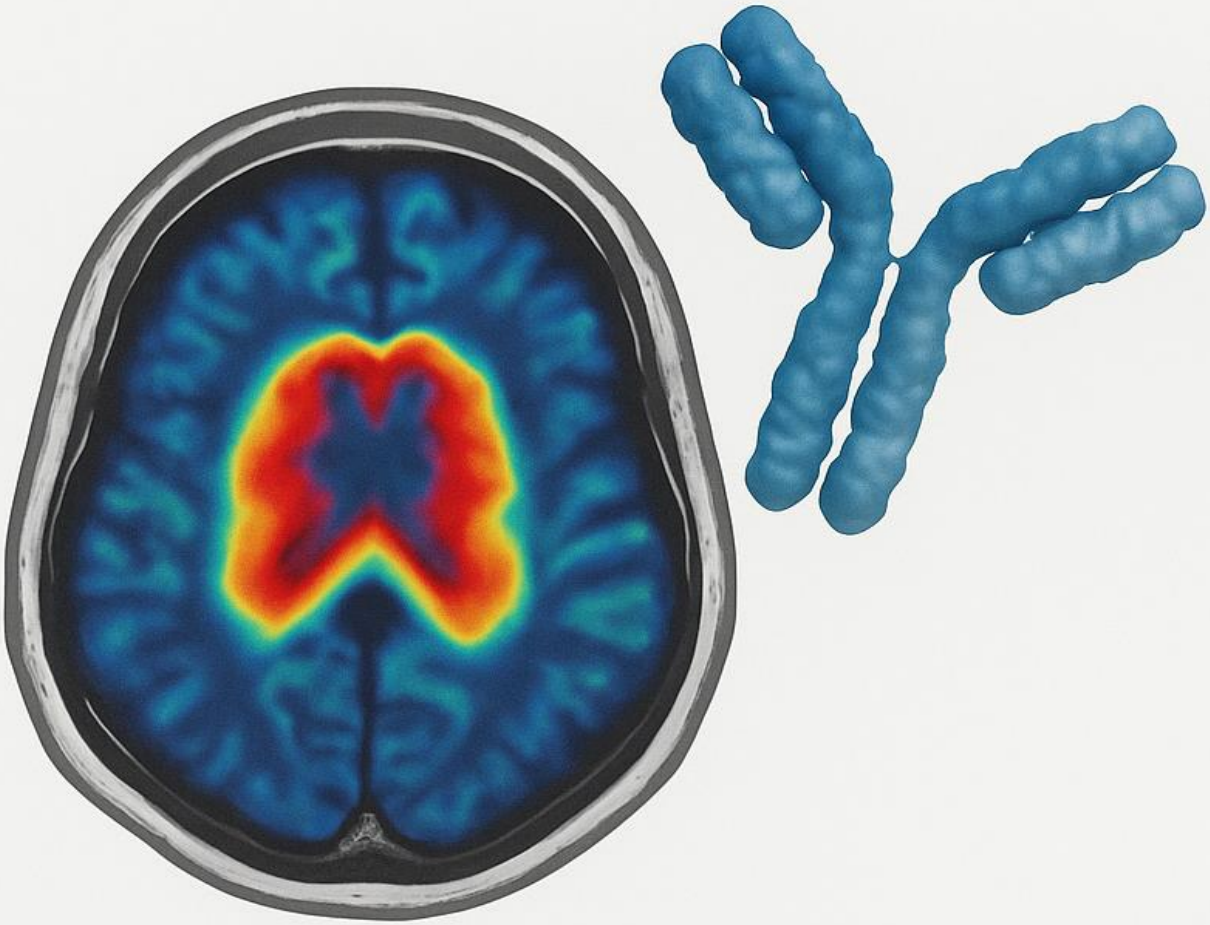

Kaylee de Jong

June 2025

BACKGROUND UPTAKE OF MONOCLONAL ANTIBODIES IN THE BRAIN

K.N. (Kaylee) de Jong

MSc Technical Medicine
Student number: 5640679
11 June 2025

Thesis in partial fulfilment of the requirements for the joint degree of Master of Science in *Technical Medicine*

Leiden University ; Delft University of Technology ; Erasmus University Rotterdam

Master thesis project (TM30004; 35 ECTS)
Department of Medical Oncology, Amsterdam UMC–location VUmc
February 2025–June 2025

Prof. Dr. W. Menke - van der Houven van Oordt	Medical supervisor
Dr. E. van de Giessen	Medical supervisor
Dr. J. Schiphof–Godart	Technical supervisor
Dr. I. Miedema	Daily supervisor

Thesis committee members:
Dr. F.H.P. van Velden, LUMC (chair)
Prof. Dr. W. Menke - van der Houven van Oordt, Amsterdam UMC
Dr. J. Schiphof–Godart, Erasmus MC

An electronic version of this thesis is available at `http://repository.tudelft.nl/`.

1 Abstract

Introduction

Monoclonal antibodies (mAbs) are increasingly used as therapeutic agents in neuro-oncology and neurodegenerative disease. Despite their growing clinical relevance, their ability to penetrate the brain remains poorly understood due to the restrictive nature of the blood–brain barrier (BBB). Positron Emission Tomography (PET) imaging with Zirconium-89 (^{89}Zr)-labeled mAbs allows for quantification of antibody uptake in organs and tumors. This study aims to quantify the baseline, non-specific uptake of ^{89}Zr-labeled mAbs in brain tissue. Additionally, the influence of target expression, BBB disruption, lesion viability, and dosing on antibody uptake was investigated.

Methods

Retrospective Positron Emission Tomography/Computed Tomography (PET/CT) data from three clinical trials with ^{89}Zr-labeled mAbs were analyzed. K_i values, representing irreversible tracer uptake, were derived using Patlak analysis from scans $\geq$1-day post-injection. Brain tissue and metastases were delineated manually, and K_i values were compared across cohorts with no target expression, target expression, and brain metastases. Interobserver reliability was assessed, and statistical comparisons were performed using Kruskal–Wallis and Wilcoxon tests.

Results

Uptake in normal brain tissue was assessed in 18 patients, two of whom had post-treatment brain metastases that were included in the analysis. Ki in target-negative brain tissue was low but measurable (median: $2.0 \times 10^{-5}\,\mu\text{L} \cdot \text{g}^{-1} \cdot \text{h}^{-1}$, IQR: $1.5 - 3.2$), indicating baseline non-specific uptake. Ki was significantly higher in target-positive brain tissue (median: $3.9 \times 10^{-5}\,\mu\text{L} \cdot \text{g}^{-1} \cdot \text{h}^{-1}$, IQR: $2.5 - 4.6$), and substantially elevated in post-treatment brain metastases (median: $120 \times 10^{-5}\,\mu\text{L} \cdot \text{g}^{-1} \cdot \text{h}^{-1}$, IQR: $115 - 180$). Notably, uptake was particularly high in post-treatment lesions with viable tumor tissue (median: $180 \times 10^{-5}\,\mu\text{L} \cdot \text{g}^{-1} \cdot \text{h}^{-1}$, $n = 2$), compared to post-treatment lesions with therapy-related imaging changes ($52.1 \times 10^{-5}\,\mu\text{L} \cdot \text{g}^{-1} \cdot \text{h}^{-1}$). In a subset of five patients with two injections with different doses of non-labeled mAb, three showed decreased Ki at higher mass doses.

Conclusion

Irreversible brain uptake of mAbs can be quantified using Patlak-derived Ki values, even at low levels. The data establish a baseline for non-specific brain uptake. The uptake is significantly higher in the presence of target expression and even higher in brain metastases, likely due to BBB disruption. These findings support the use of PET imaging with Patlak analysis as a non-invasive method to evaluate CNS target engagement and drug delivery in early-phase clinical trials

Contents

1 Abstract **1**

2 Introduction **3**

3 Methods **4**
- 3.1 Data Collection . . . 4
- 3.2 Image Acquisition . . . 4
- 3.3 Biodistribution Analysis . . . 4
- 3.4 Blood Sampling . . . 4
- 3.5 Patlak Analysis . . . 5
- 3.6 Primary outcome measurements . . . 6
- 3.7 Statistical analysis . . . 6

4 Results **8**
- 4.1 Patient characteristics . . . 8
- 4.2 Delineation of brain tissue . . . 8
- 4.3 Inclusion and Evaluation of Patlak Data . . . 9
- 4.4 Quantification of Irreversible Brain Uptake . . . 11
- 4.5 Comparison of Uptake Between Viable and TRIC Lesions . . . 13
- 4.6 Evaluation of Target Saturation Across Sequential Injections . . . 14

5 Discussion **15**
- 5.1 Irreversible Uptake in Target-Negative Tissue . . . 15
- 5.2 Irreversible uptake in Target-Positive tissue . . . 16
- 5.3 Irreversible uptake in brain metastases . . . 16
- 5.4 Saturation effect . . . 17
- 5.5 Comparison with published Ki values in brain tissue . . . 17
- 5.6 Strong points and limitations . . . 17
- 5.7 Future research . . . 18
- 5.8 Clinical implications . . . 19

6 Conclusion **20**

7 Supplementary **25**
- 7.1 Supplementary, Tables . . . 25
- 7.2 Supplementary Figure 1, study with mAb 1 . . . 27
- 7.3 Supplementary Figure 2, study with mAb 2 . . . 33
- 7.4 Supplementary Figure 3, HER2 study no metastases . . . 36
- 7.5 Supplementary Figure 4, HER2 study metastases . . . 38

2 Introduction

Monoclonal antibodies (mAbs) are increasingly used as therapeutic agents across oncology and neurology. However, a major challenge in central nervous system (CNS) drug development is determining whether the antibody reaches its intended site of action within the brain. The blood–brain barrier (BBB) poses a substantial obstacle for large molecules such as mAbs, severely limiting their penetration into brain parenchyma under physiological conditions. Although the human brain microvasculature spans a surface area of approximately 20 m^2, it is estimated that only 0.1–0.2% of a systemically administered mAb dose crosses the BBB (Jones & Shusta, 2007; Pardridge, 2016b).

In humans, slightly higher values (0.5–1.5%) have been reported for anti-amyloid antibodies, but these estimates are based on concentrations measured in cerebrospinal fluid (CSF), which may overestimate brain parenchymal uptake due to contributions from the more permeable blood-CSF barrier (Tolar et al., 2020). The true fraction reaching brain tissue is likely even lower (Pardridge, 2016a). This severely limits therapeutic exposure in the CNS and often necessitates high or repeated dosing, increasing the risk of toxicity and immunogenicity (Kouhi et al., 2021). These low uptake values apply to intact BBB conditions. In pathological states such as brain metastases, the BBB and blood–tumor barrier (BTB) may be disrupted, enabling higher mAb penetration. This has been observed both in untreated lesions and particularly following radiotherapy, where transient or localized increases in permeability have been reported (Sprowls et al., 2019).

Positron Emission Tomography (PET) imaging with Zirconium-89 (^{89}Zr)-labeled mAbs allows non-invasive assessment of antibody distribution in the body (Heskamp et al., 2017). A common approach is to calculate standardized uptake values (SUVs), which reflect the total tracer concentration in a tissue at a single time point. However, SUV does not distinguish between reversible and irreversible uptake, nor does it account for differences in plasma tracer concentration (Boellaard, 2009). To overcome these limitations, kinetic modeling approaches such as Patlak analysis are used. Patlak analysis separates reversible uptake (such as tracer present in the blood or interstitial space) from irreversible uptake (K_i), which reflects tracer that is internalized and retained within tissue — either via target-mediated mechanisms or non-specific catabolism (Patlak et al., 1983). This enables quantification of true tissue accumulation, even in regions with low uptake.

Despite growing interest in CNS-targeted antibody therapies, baseline antibody uptake in healthy brain tissue remains poorly defined. The primary aim of this study was to objectively determine the non-specific, baseline uptake of antibodies in brain tissue in the absence of target expression. In addition, we explored how tracer uptake is affected by biological factors such as target presence, BBB disruption due to brain metastases, and lesion viability (viable tissue vs. tissue with therapy-related imaging changes). Finally, we assessed whether increasing antibody dose would lead to reduced tracer uptake, which may indicate target-mediated saturation. Irreversible uptake was quantified using Patlak analysis of ^{89}Zr-PET/CT data across three distinct patient cohorts.

3 Methods

3.1 Data Collection

Retrospective data from clinical imaging studies conducted at Amsterdam UMC, location VUmc were collected. Studies were selected based on the following criteria:

1. Availability of large field of view Quadra PET/CT scans with an ^{89}Zr-labeled therapeutic mAb,
2. Availability of plasma activity concentrations derived from venous blood samples collected at each imaging time point, and
3. Availability of scans at multiple time points (at least two >1 day after injection of ^{89}Zr mAb).

All studies were approved by the Medical Ethics Review Committee of Amsterdam University Medical Centers, and written informed consent was obtained from all participants. The included studies are shown in Table 1. For further details on study design, see the respective publications.

3.2 Image Acquisition

All PET scans were acquired using a Biograph Vision Quadra large field of view PET/CT scanner (Siemens Healthineers, Erlangen, Germany) at Amsterdam UMC, location VUmc. A low-dose CT scan (ldCT) was performed to correct for scatter, dead time, randoms, radioactive decay, and tissue attenuation of the PET data. CT images were co-registered with the PET data to ensure accurate spatial alignment of anatomical and functional information.

3.3 Biodistribution Analysis

The ldCT and PET scans were analyzed using the in-house BIODISTRIBUTION software tool (developed in IDL, version dated 25-05-2023) (Boellaard, 2018a). Brain tissue was manually delineated on each scan. Blood vessels and any brain metastases were excluded from the delineation. Brain metastases were delineated separately using the in-house ACCURATE tool (developed in IDL, version dated 10-07-2024) (Boellaard, 2018b). For each volume of interest (VOI), the mean radioactivity concentration was determined in Becquerel per mL (Bq/mL), representing the tissue activity concentration (ACt) used in the Patlak analysis. Activity concentrations were decay-corrected to the time of injection.

For each antibody, the Human Protein Atlas was used as a reference to assess the presence or absence of target antigen expression at the protein level in the brain (Uhlen et al., 2010).

3.4 Blood Sampling

Venous blood samples were collected as part of previously conducted clinical studies, and these data were used in the present retrospective analysis (Table 1). Samples were separated into cells and plasma, and tracer concentration in the plasma fraction was measured using a cross-calibrated well counter. Radioactivity concentrations were expressed as activity per liter relative to the injected activity (%IA/L).

3.5 Patlak Analysis

In tissue without target expression, the activity concentration in tissue (ACt) reflects both reversible and irreversible components of tracer uptake, such as catabolism (Equation 1). Patlak analysis enables separation and quantification of these two components, under the assumption that equilibrium between the plasma concentration and unbound tracer in tissue has been reached–typically after 24 hours for mAbs (Patlak et al., 1983; Wijngaarden et al., 2022). Therefore, only imaging time points from one day after injection and later were included in the analysis, as equilibrium is not expected to be established earlier.

In the Patlak model, reversible uptake is proportional to the current supply of mAbs, which is the activity concentration in plasma (ACp). The irreversible uptake is proportional to the supply of mAbs accumulated over time, which is the area under the plasma curve from the injection time to the time of measurement (AUCp) (Equation Equation 2). Normalizing all terms to plasma activity concentration (ACp) yields a linear relationship, known as the Patlak equation (Equation Equation 3).

$$AC_T = \text{reversible uptake} + \text{irreversible uptake} \quad \text{(Equation 1)}$$

$$AC_T = AC_P + AUC_P \quad \text{(Equation 2)}$$

$$\frac{AC_T}{AC_P} = K_i \times \frac{AUC_P}{AC_P} + V_T \quad \text{(Equation 3)}$$

Patlak plots were generated using the measured activity concentrations in plasma and tissue at multiple time points following the ^{89}Zr-mAb injection. The x-axis represents the ratio of cumulative plasma activity to current plasma activity (AUC_p/AC_p) and the y-axis represents the ratio of tissue to plasma activity (AC_t/AC_p). The slope of the linear fit corresponds to K_i, the net influx rate of tracer from plasma into tissue (irreversible uptake, in $mL \cdot g^{-1} \cdot min^{-1}$ or h^{-1}). The y-intercept of the plot reflects V_T, an approximation of the distribution volume, which represents reversible uptake (in $mL \cdot cm^{-3}$) (Patlak et al., 1983).

Patlak analysis was performed to quantify the irreversible uptake of the tracer in brain tissue. In the absence of target expression in the brain, K_i was assumed to reflect non-specific, irreversible retention of the antibody. This may include cellular processes such as phagocytosis by microglia or non-specific endocytosis by resident brain cells (e.g., astrocytes or endothelial cells), followed by intracellular catabolism that traps the radiolabel within the cell. This allowed us to characterize the baseline level of irreversible brain uptake in the absence of target-mediated binding.

In Patlak analysis, it is assumed that the tracer is irreversibly taken up by the target tissue, implying that there is no significant efflux back into the plasma. For brain tissue, however, it is uncertain whether this assumption always holds, as characteristics of antibody uptake in brain are not well established. To explore irreversible uptake, a Patlak plot was generated for each patient and each injection, using two or three data points corresponding to the available imaging timepoints (Supplementary Figure 7.2).

For plots based on three time points, the quality of the linear fit was first assessed using the coefficient of determination (R^2). Only plots with $R^2 \geq 0.9$ were included for further evaluation. For these, as well as for all two-point plots (where $R^2 = 1$ and thus not informative), K_i was retained if positive. If K_i was negative but decreased by less than 10%, assuming that this is still within the noise range, the data point was included, and K_i was set to zero. If the decrease exceeded 10%, the data point was excluded, as negative K_i values were considered physiologically implausible and inconsistent with the assumptions of the Patlak model. In two-point plots, linearity was assumed, as it could not be formally assessed.

3.6 Primary outcome measurements

K_i values were calculated per injection per patient. Within each study, these values were then summarized as medians with interquartile ranges (IQR). For the no target and brain metastasis groups, the median K_i was first calculated per study or per patient, respectively. The mean of these medians was then reported as the representative K_i for each group. For the target group, the median K_i across all patients in the single available study was used.

The subdivision of brain metastases into therapy-related imaging changes (TRIC) and viable lesions aimed to distinguish between passive tracer leakage and potential target-specific uptake. This classification was based on serial follow-up MRI. Lesions that showed an increase in volume over time were classified as viable, whereas lesions that remained stable in size and exhibited no MRI signs of tumor progression were classified as TRIC.

K_i values were stratified into three groups:

1. Antibodies with no known target expression in the brain (target 1 and HER2)
2. Antibodies with expected target expression in the brain (target 2)
3. Patients with HER2-positive breast cancer and (previously irradiated) brain metastases (HER2-004 and HER2-008):
   (a) Post-treatment lesions with TRIC
   (b) Post-treatment lesions with viable tumor tissue

In patients who received two injections of the same radiolabeled antibody, each combined with a different mass dose of unlabeled (cold) antibody, K_i values were directly compared to assess potential target saturation. A lower K_i after the higher cold mass dose may indicate saturation of target-mediated uptake.

3.7 Statistical analysis

To assess differences in K_i between these three groups, a Kruskal–Wallis test was performed. This non-parametric test was selected due to the small sample sizes, non-normal distribution of the data, and the comparison of more than two independent groups. In addition, pairwise Wilcoxon rank-sum tests (with Benjamini–Hochberg correction) were performed to explore differences between two groups (3a and 3b). A p-value < 0.05 was considered statistically significant. Statistical tests were performed in RStudio (version 4.4.3) (RStudio Team, 2025).

Each scan was manually delineated by two independent raters. One rater remained consistent across all studies, while the second rater varied per study. Interobserver variability was assessed using intraclass correlation coefficients (ICC), calculated via a two-way mixed-effects model with absolute agreement. To estimate the overall interobserver reliability across studies, a random-effects meta-analysis was performed on the study-specific ICCs, resulting in a pooled ICC with a corresponding 95% confidence interval. For the interpretation of the ICCs, the standard thresholds were used: ≥ 0.90 is excellent, ≥ 0.75 is good, ≥ 0.50 is moderate and < 0.50 is poor (Mary & Watkins, 2008).

Table 1: Overview of ^{89}Zr-Immuno-PET studies

^{89}Zr-Immuno-PET tracer	**[^{89}Zr]Zr-mAb 1**	**[^{89}Zr]Zr-trastuzumab**	**[^{89}Zr]Zr-mAb 2**
mAb	mAb 1	trastuzumab	mAb 2
Target of antibody	CD137 and FAP (bispecific)	HER2	SIRP-alpha
Chelator	DFO	DFO*	DFO
Antibody isotype	IgG1	IgG1	IgG1
Target expression in brain(Uhlen et al., 2010)	Absent	Absent	Present
Tumor type	Advanced solid cancer	Gastric or breast cancer	NSCLC*, HNSCC**, or melanoma
Number of patients	8	6	4
Hot mAb mass dose	Low	50 mg	Low
Injected activity	37 MBq	37 MBq	37 MBq
PET scan time points (p.i.)	**pt 1–4:** 1–2 h***, 1 d, 2 d, 3 d **pt 5,6,8,10:** 1 d, 3 d, 6 d	1–2 h*** 1 d, 4 d, 6 d	1–2 h 1 d 2 d
Blood sampling time points (p.i.)	30 min 1 h 2 h 6 h (Cycle 1) or 8 h (Cycle 2)	10 min 30 min 1 h 2 h Each PET scan	10 min 30 min 1 h 2 h 4 h
Reference	NCT03922204	NCT05955833	NCT05737628

* Non-Small Cell Lung Carcinoma
** Head and Neck Squamous Cell Carcinoma
*** Three patients underwent an additional scan 1–2 hours p.i. for dosimetry purposes

4 Results

4.1 Patient characteristics

A total of 18 patients were included and categorized into three groups based on brain target expression and the presence of brain metastases: group 1 (no target, no brain metastases, n = 12), group 2 (target expression in brain tissue, n = 4), and group 3 (no target, but presence of brain metastases, n = 2). Median age was 68 years (range: 27–72) in group 1, 56 years (range: 46–68) in group 2, and 49 years (range: 43–54) in group 3. Baseline patient characteristics are listed in Table 2.

Group	**N**	**Antibody**	**Median age (range)**
No target expression, no metastases	12	8x mAb 1+ 4x trastuzumab	67.5 (27 – 72)
Target expression in brain	4	4x mAb 2	55.5 (46 – 68)
No target expression, brain metastases	2	2x trastuzumab	48.5 (43 – 54)

Table 2: Overview of patient characteristics per group. Patient groups were defined based on presence of target expression in the brain and presence of brain metastases. For each group, the number of patients, administered antibody type, and median age (range) are shown.

4.2 Delineation of brain tissue

On all PET/CT scans, brain tissue was manually delineated using the in-house BIODISTRIBUTION tool. Blood vessels, visible brain metastases, and the choroid plexus were excluded. The ventricular system was not excluded, as it was not clearly visible on the low-dose CT scans. When present, brain metastases were delineated separately using the ACCURATE tool. Examples of brain and tumor delineations on CT and PET are shown in Figure 1. Inter-observer agreement for brain tissue delineation was excellent, with ICCs of 0.966 for the study with mAb 1, 0.994 for the study with mAb 2 and 0.963 for the HER2 study.

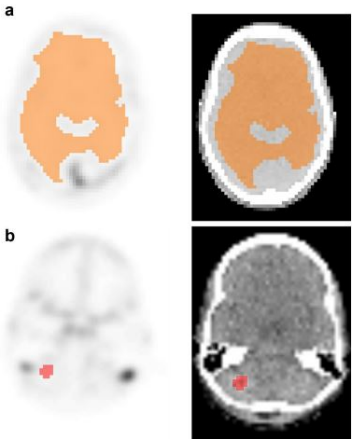

Figure 1: a) Brain tissue delineation shown on low-dose CT (right) and corresponding PET image (left). Regions with uptake in the choroid plexus and in a brain metastasis were excluded. (b) Delineation of a brain metastasis using the ACCURATE tool, shown on PET (left) and low-dose CT (right).

4.3 Inclusion and Evaluation of Patlak Data

Patlak linearization was conducted for each patient and injection, and additionally per metastasis if present. In total, 30 injections were analyzed across the three studies: 16 in the study with mAb 1 (8 low-dose and 8 high-dose), 8 in the study with mAb 2 (4 low-dose and 4 high-dose), and 6 in the HER2 study, all administered at a 50 mg dose.

In the study with mAb 1, 8 patients received two injections each. In 4 patients, all three PET scans were available for analysis. In 3 others, only two scans were used due to early acquisition of the first scan ($<$ 1 day post-injection). In one patient, a scan was excluded due to missing blood data, also leaving two usable scans. Of the 16 injections, 9 had an $R^2 > 0.9$. Eight of these showed an upward trend in the Patlak plot, while one decreased slightly (1.3%) and the corresponding K_i was set to zero.

Examples of Patlak plots representing different classification outcomes (positive K_i, K_i set to zero, and exclusion due to $>$ 10% slope decrease) are shown in Figure 2.

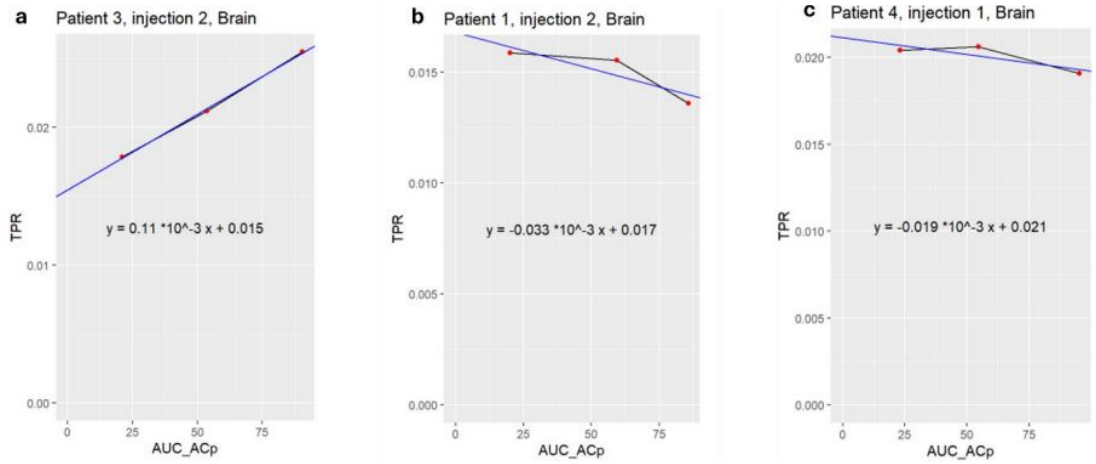

Figure 2: a) Patient with an increasing trend in tracer uptake, meeting criteria for inclusion.
b) Patient with a decreasing trend greater than 10%, excluded from analysis.
c) Patient with a decreasing trend smaller than 10%, included in analysis. .

In the study with mAb 2, four patients received two injections (8 total). For four injections, three PET scans were available. The remaining four were based on two scans due to early acquisition of the first scan ($<$ 1 day post-injection). One injection was excluded due to an $R^2 < 0.9$. Of the remaining seven, four showed an increasing trend and three a decreasing trend, all under the 10% threshold.

In the HER2 study, six patients received one injection each. For one patient, blood data were missing at two of the three imaging time points, leaving only a single usable data point. As at least two time points are required to perform Patlak analysis, neither K_i nor R^2 could be determined for this patient. In the remaining five patients, all three PET scans were available. Of these, only one case – belonging to the no-target group – showed an $R^2 > 0.9$ and yielded a positive K_i.

Two patients in the HER2 study had brain metastases. One had a single lesion classified as TRIC (radionecrosis). The other had five lesions: three TRIC and two viable. Of the six lesions in total, three had an $R^2 > 0.9$ and showed a positive K_i. These included one TRIC lesion (patient 4) and two viable metastatic lesions (patient 8) (Figure 3).

Across all studies, a total of 30 injections were administered (16 mAb 1, 8 mAb 2, 6 HER2). R^2 and K_i could be calculated for 29 of these injections; one was excluded due to insufficient data (only one usable time point). In total, 35 Patlak analyses were performed: 29 at the injection level (one per injection) and 6 at the lesion level in patients with brain metastases (multiple lesions per injection). Of these 35 datasets, 27 were based on three PET scans and eight on two. Fifteen values with $R^2 < 0.9$ were excluded from further analysis. One K_i value with $R^2 > 0.9$ was set to zero due to a decrease in slope ($< 10\%$).

After applying these criteria, 20 of 35 K_i values (57.1%) were retained for evaluation: 9 of 16 for mAb 1, 7 of 8 for mAb 2, 1 of 6 for HER2 (whole-brain), and 3 of 6 for brain metastases (lesion-level). An overview of all R^2 and K_i values is provided in (Supplementary Table 4).

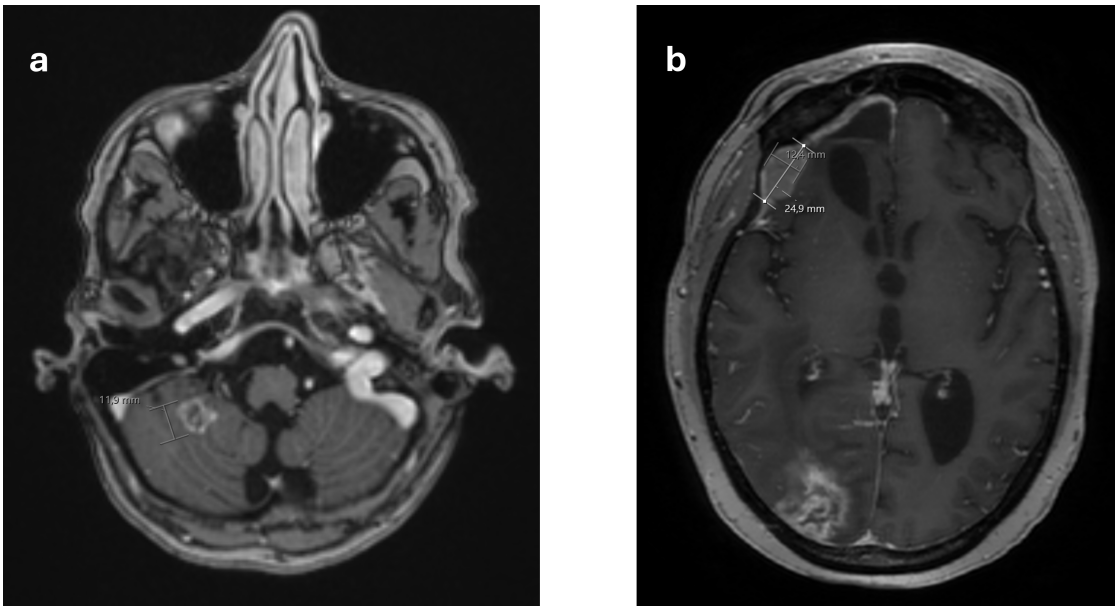

Figure 3: (a) Axial contrast-enhanced T1-weighted image of Patient 4, showing a cerebellar lesion classified as TRIC (therapy-related imaging changes). (b) Axial contrast-enhanced T1-weighted image of Patient 4, showing a cerebellar lesion classified as TRIC (therapy-related imaging changes of Patient 8, showing a viable brain metastases in the right frontal lobe.

4.4 Quantification of Irreversible Brain Uptake

Irreversible uptake is reflected by a positive K_i value, which was the case in 19 out of 20 analyzed injections (95%). When the antibody does not have a brain target, K_i reflects non-specific irreversible uptake, interpreted as background uptake. For mAb 1 and HER2 tracers, the median K_i values were 2.6×10^{-5} (IQR: 1.9×10^{-5} – 3.4×10^{-5}) and 1.4×10^{-5} $\mu\text{L} \cdot \text{g}^{-1} \cdot \text{h}^{-1}$, respectively.

In the presence of a target, K_i increased to a median of 3.9×10^{-5} (IQR: 2.5×10^{-5} – 4.6×10^{-5}). When a post-treatment brain metastasis was present, the K_i further increased to 120×10^{-5} $\mu\text{L} \cdot \text{g}^{-1} \cdot \text{h}^{-1}$. In viable tumor tissue, K_i reached 180×10^{-5}, while in TRIC lesions it was 5.2×10^{-5} $\mu\text{L} \cdot \text{g}^{-1} \cdot \text{h}^{-1}$. Values for K_i per group are summarized in Table 3.

Table 3: Irreversible uptake (Ki) values per patient group and antibody.

Group	**Ki**
No target	$2{,}0 \times 10^{-5}$ ($1{,}5 \times 10^{-5}$ – $3{,}2 \times 10^{-5}$)
mAb1	$2{,}6 \times 10^{-5}$ ($1{,}9 \times 10^{-5}$ – $3{,}4 \times 10^{-5}$)
HER2	$1{,}4 \times 10^{-5}$
Target	$3{,}9 \times 10^{-5}$ ($2{,}5 \times 10^{-5}$ – $4{,}6 \times 10^{-5}$)
Brain metastasis	120×10^{-5}(115×10^{-5} – 180×10^{-5})
Post treatment TRIC lesions	52×10^{-5}
Post treatment lesions with viable tumor tissue	180×10^{-5}

These group differences are visualized in Figure 4. A Kruskal–Wallis test showed a significant overall difference between the three groups ($p = 0.009$), with post-hoc comparisons showing significantly higher uptake in the brain metastasis group compared to both the no-target ($p = 0.021$) and target ($p = 0.036$) groups.

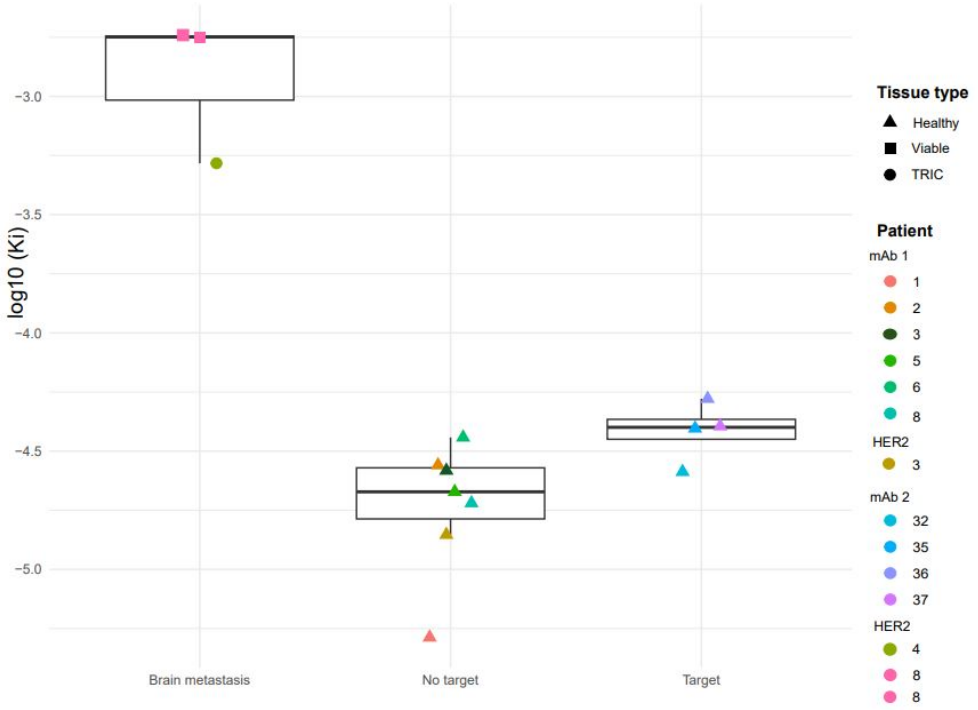

Figure 4: Boxplot of K_i values ($\mu\text{L} \cdot \text{g}^{-1} \cdot \text{h}^{-1}$) in normal brain tissue without target expression ("no target" group), normal brain tissue with target expression ("target" group), and post-treatment brain metastases. Each box represents the interquartile range (IQR), with the median indicated by the central line. Whiskers represent 1.5 times the IQR. K_i values reflect non-specific background uptake in the non-target group, and both non-specific and specific irreversible uptake in the target and metastasis groups. **TRIC** = therapy-related imaging changes.

4.5 Comparison of Uptake Between Viable and TRIC Lesions

Figure 5 shows the K_i values measured in brain lesions of two patients. The measured K_i value in the TRIC lesion of patient 4 was 52.1×10^{-5} $\mu\text{L} \cdot \text{g}^{-1} \cdot \text{h}^{-1}$. The two viable brain metastases of patient 8 showed K_i values of 178.2×10^{-5} and 181.6×10^{-5} $\mu\text{L} \cdot \text{g}^{-1} \cdot \text{h}^{-1}$, with a mean of 180×10^{-5} $\mu\text{L} \cdot \text{g}^{-1} \cdot \text{h}^{-1}$. The difference between the average uptake in viable metastases and the TRIC lesion was 127.9×10^{-5} $\mu\text{L} \cdot \text{g}^{-1} \cdot \text{h}^{-1}$.

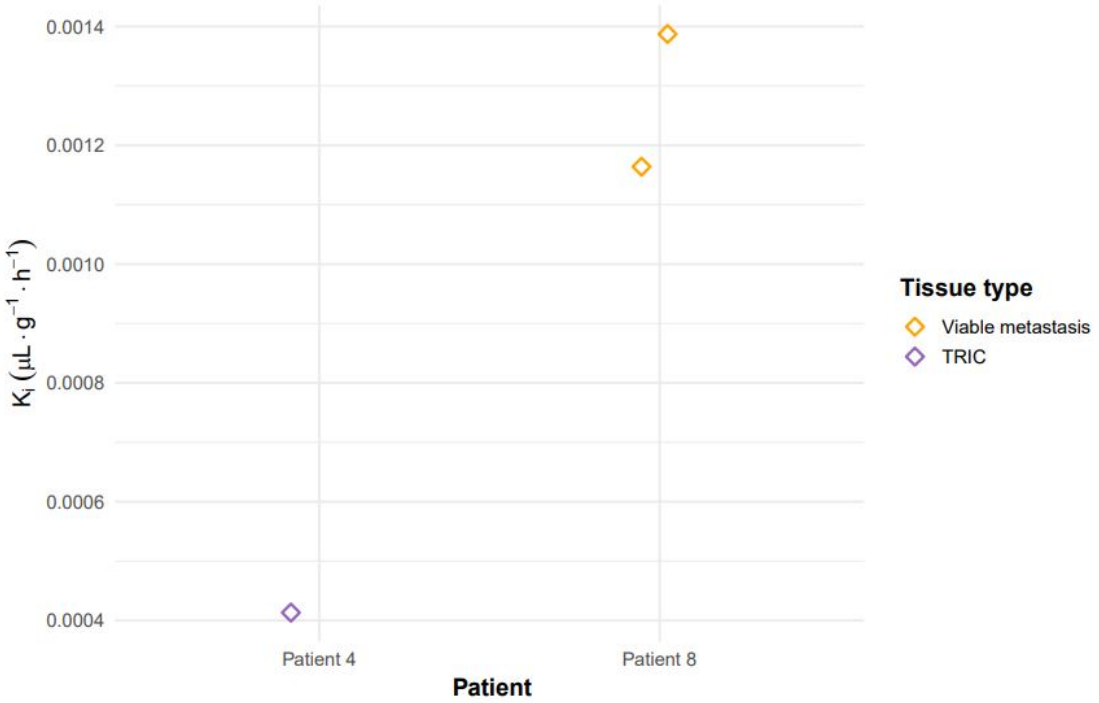

Figure 5: K_i values ($\mu\text{L} \cdot \text{g}^{-1} \cdot \text{h}^{-1}$) measured in one TRIC lesion (Patient 4) and two viable brain lesions (Patient 8). Lesions are color-coded by tissue type.

4.6 Evaluation of Target Saturation Across Sequential Injections

In two of the three included studies, patients received two sequential injections, allowing evaluation of potential target saturation effects. Saturation was assessed by comparing K_i values between the first (low cold mass dose) and second injection(high cold mass dose). Only patients with reliable Patlak-derived values ($R^2 > 0.9$ and $K_i > 0$) at both injection time points were included. This resulted in two evaluable patients for the study with mAb 1 and three for the study with mAb 2.

In the study with mAb 1, one patient showed an increase in K_i after the second injection (from 2.62×10^{-5} to 11.0×10^{-5}), while another patient showed a decrease (from 1.91×10^{-5} to 0.293×10^{-5}). In the study with mAb 2, K_i increased in one patient (from 3.95×10^{-5} to 5.38×10^{-5}) and decreased in the other two patients (from 2.58×10^{-5} to 0 and from 4.03×10^{-5} to 2.49×10^{-5}).

No consistent change in K_i between the first and second injection was observed across patients.

Figure 6 illustrates the individual K_i values per injection, allowing visual comparison of uptake changes between the first and second administration.

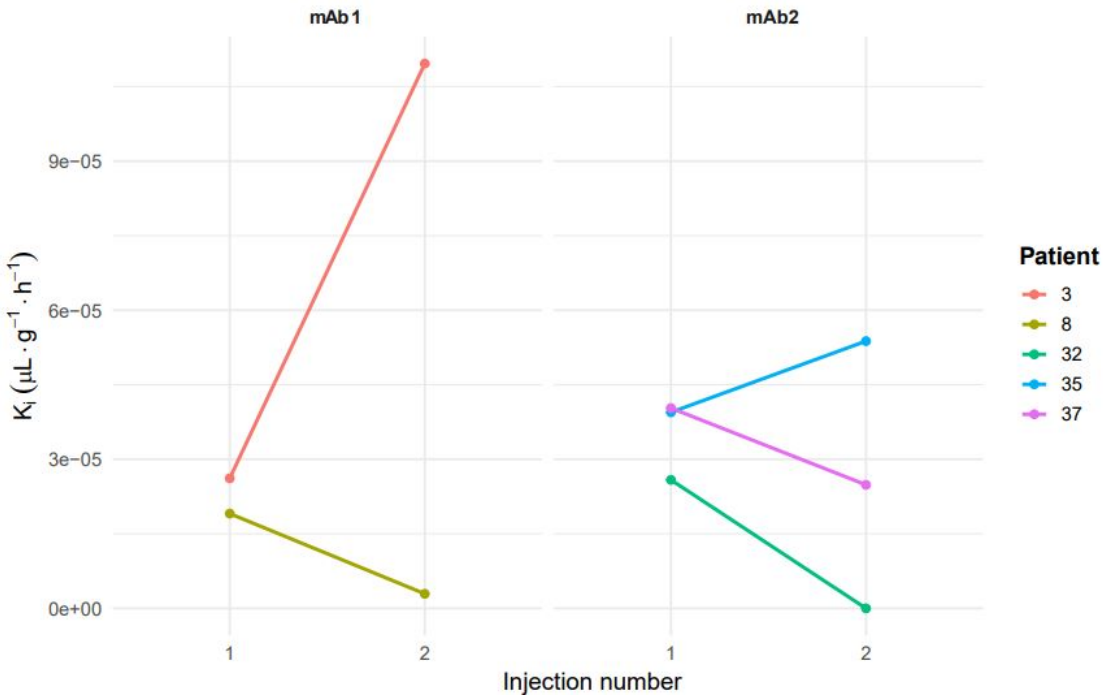

Figure 6: K_i values ($\mu\text{L} \cdot \text{g}^{-1} \cdot \text{h}^{-1}$) per patient after two sequential injections in the studies with mAb 1 and mAb 2. Each line connects the K_i values from injection 1 and 2 for the same patient.

5 Discussion

This study demonstrates that Patlak analysis can detect and quantify irreversible uptake of antibodies in the brain, even when the uptake is low. The lowest Ki values were observed in the no-target group, reflecting baseline non-specific irreversible uptake. In the group with target expression but intact BBB, significantly higher Ki values (60-fold) were already detected, indicating that specific target-mediated uptake can be detected and distinguished from background signal, even without BBB disruption. Notably, substantially higher Ki values were found in post-treatment brain metastases where BBB integrity was compromised. Within this group, uptake was higher in viable lesions compared to TRIC lesions. Together, these findings underscore the substantial impact of BBB permeability on antibody uptake in brain tissue.

5.1 Irreversible Uptake in Target-Negative Tissue

In 85.7% (18/21) of injections in the no-target group, K_i values above zero were observed, indicating measurable irreversible uptake of ^{89}Zr-labeled antibodies in brain tissue. This reflects the non-specific baseline uptake in the absence of target engagement. Multiple biological, physiological, and technical factors may contribute to this signal.

A key biological mechanism is the intracellular degradation of antibodies in brain endothelial cells and the residualizing nature of ^{89}Zr. Without neonatal Fc receptor (FcRn)-mediated recycling, internalized antibodies are trafficked to lysosomes, where ^{89}Zr remains trapped after degradation (Heskamp et al., 2017; Pyzik et al., 2019). This leads to irreversible signal retention, particularly in capillary endothelium. While large vessels were excluded during VOI delineation, capillaries cannot be reliably segmented and likely contribute to the observed uptake. This uptake likely reflects physiological antibody catabolism in brain tissue that has no target expression. Another mechanism is immune-mediated clearance. Antibodies that cross the BBB in small amounts may bind to Fc-gamma (Fc-γ) receptors on microglia, leading to internalization and catabolism, independent of target binding (Mellman & Plutner, 1984). A third contributor may be low-affinity off-target binding. Despite high target specificity, mAbs can interact with non-target proteins, resulting in internalization and non-specific tissue retention (Bumbaca et al., 2011).

In addition to true biological uptake, technical and physiological factors may overestimate K_i.Limited PET resolution ($\sim$ 4–5 mm) causes partial volume effects, leading to spill-in from nearby vessels (Watakabe et al., 2020). The brain's vascular volume ($\sim$ 3–5%) and slow antibody clearance can also cause prolonged intravascular signal.Although this signal is reversible, it may contaminate the tissue VOI, especially if blood correction is imperfect (Leenders et al., 1990). Inaccuracies in blood or tissue signal can affect K_i estimates in any tissue, but their impact is greater in low-uptake regions like the brain. Even small deviations can result in negative K_i values, which are physiologically implausible.However, excluding them would bias the data upward. Therefore, small decreases (up to $\sim$ 10%) were considered acceptable and likely reflect noise rather than true efflux (Jauw et al., 2018).

These findings show that even in the absence of target expression, small but measurable irreversible uptake of ^{89}Zr-labeled antibodies can be detected in brain tissue. However, in low-uptake conditions, Patlak analysis becomes more sensitive to variability. When irreversible tracer retention is minimal, signal-to-noise ratios (SNRs) are low, which can compromise the linearity of the fit, as observed in 5 out of 6 patients in the HER2 group.

This underlines that while Patlak modeling can be applied in the brain, its reliability is limited in settings where tracer retention is minimal and SNR is poor. Then, even small fluctuations in signal can compromise the quality of the linear fit and the accuracy of the estimated K_i.

5.2 Irreversible uptake in Target-Positive tissue

In contrast to target-negative tissue, irreversible uptake in target-positive tissue is at least partly driven by specific antibody–target interactions. mAb 2, used in the mAb 2 study, binds to a receptor which is mainly expressed on microglia, which are resident immune cells making up 0.5–16.6% of brain cells (Bachiller et al., 2018). Upon binding, the antibody–receptor complex is internalized and degraded in lysosomes. Since ^{89}Zr is residualizing, it remains trapped intracellularly, resulting in irreversible signal accumulation detectable by PET (Heskamp et al., 2017).

The higher K_i values observed in the target-positive group support selective antibody retention via target engagement. This aligns with the high affinity of mAb 2 for its target. However, affinity alone is unlikely to fully account for the observed uptake. Target density and availability also play a role. In the case of mAb 2, interindividual differences in microglial abundance and activation state may influence receptor expression levels, thereby modulating antibody uptake (Wang, 2025).

5.3 Irreversible uptake in brain metastases

Irreversible uptake in brain metastases was substantially higher than in both the target and no-target groups—approximately 29-fold and 58-fold, respectively. This likely reflects disruption of the BBB, which is common in viable brain metastases and TRIC lesions, and was visible on contrast-enhanced MRI scans of the patients. The BBB disruption allows antibodies to extravasate more readily than in healthy tissue, where the BBB limits access to the interstitial space (Keaney & Campbell, 2015; Arvanitis et al., 2020).

Within the post-treatment metastases, K_i values were markedly higher in viable lesions with viable tumor tissue compared to the TRIC lesion — on average 3.45 times higher. Viable lesions are vascularized and contain HER2-expressing tumor cells, enabling trastuzumab binding, internalization, and ^{89}Zr retention (Dewhirst & Secomb, 2017; Pereslete et al., 2025). In addition to specific binding, some degree of non-specific uptake likely occurs through antibody catabolism, as previously described for target-negative tissue. Tumor-intrinsic factors such as oncogene-driven inflammation may further enhance vascular permeability and antibody delivery (Hibino et al., 2021). Thus, uptake in viable lesions likely reflects a combination of non-specific catabolism, target-specific binding, and inflammation- enhanced delivery.

TRIC lesions lack viable tumor cells and thus do not support specific binding (Klemm et al., 2024). Yet, K_i values were much higher than in healthy target-positive tissue. This uptake is likely explained by local BBB disruption and sterile inflammation in the peri-necrotic rim — the peripheral zone surrounding the necrotic core of the lesion. This peripheral zone remains vascularized and may show increased permeability (Chen & Nuñez, 2010). Tracer accumulation was typically localized to the lesion rim, consistent with rim-enhancing patterns observed in treatment-related necrosis (Figure 7) (Forster et al., 2017). Central necrotic regions showed little to no uptake, reflecting poor perfusion and lack of viable tissue.

5.4 Saturation effect

In a small subgroup of five patients who received two injections at different cold mass doses, changes in K_i were evaluated to explore potential receptor saturation. Four patients received the maximum therapeutic dose at the second injection, at which at least partial saturation was expected. In three of these patients (75%), a decrease in K_i was observed, suggesting a possible saturation effect due to competition between the therapeutic and radiolabeled antibody.

However, two patients showed an increase in K_i, and overall, no consistent pattern of change was observed across the group. Therefore, while the reduced K_i in some individuals may reflect partial receptor saturation, this interpretation remains uncertain. Variation in K_i could also be influenced by biological or technical variability between time points. Given the small sample size and heterogeneity of responses, these findings should be interpreted with caution.

5.5 Comparison with published Ki values in brain tissue

A previous study investigating the brain uptake of ^{89}Zr-labeled mAbs without a target reported K_i values close to zero, ranging from 0.0 to 10.0×10^{-5} h^{-1} across a wide range of mass doses, with no evidence of dose-dependent saturation (Miedema et al., 2023). These findings confirm that, under intact BBB conditions and in the absence of target expression, antibody penetration into the brain is minimal, though not entirely absent. In the present study, K_i values in patients without a brain target were similarly low (2.0×10^{-5} h^{-1}), supporting the notion of limited non-specific uptake. Slightly higher K_i values were observed in patients with a known brain target (3.9×10^{-5} h^{-1}). In comparison, patients with brain metastases showed markedly elevated K_i values, particularly in viable tumor tissue (180×10^{-5} h^{-1}), and to a lesser extent in TRIC lesions (54×10^{-5} h^{-1}). These findings are consistent with existing literature, suggesting that disruption of the BBB in brain metastases permits greater tracer accumulation, especially in viable tumor tissue (Arvanitis et al., 2020).

5.6 Strong points and limitations

A key strength of this study is the use of Patlak analysis to quantify irreversible antibody uptake in brain tissue. Unlike standardized uptake value (SUV), which reflects total signal at a single time point and does not account for plasma activity, K_i incorporates the blood input function and measures irreversible tracer accumulation over time (Wijngaarden et al., 2023). This makes K_i particularly valuable in settings with low uptake or slow kinetics, where SUV may be confounded by background noise or circulating tracer (Cai et al., 2024). Another strength is the high interobserver agreement for brain VOI delineation, with intraclass correlation coefficients ranging from 0.83 to 0.96 across studies, indicating good to excellent reproducibility (Mary & Watkins, 2008). Moreover, the inclusion of diverse patient groups allowed comparison of uptake under different biological conditions. Scanning was performed on a state-of-the-art large field of view PET/CT system, offering very high sensitivity and image quality (Pommranz et al., 2025). This study also has limitations. Most notably, the small sample size reduces statistical power and limits generalizability. Second, BBB integrity was not directly assessed, limiting interpretation of elevated K_i values in lesions, although contrast-enhanced MRI confirmed BBB disruption in the post-treatment metastases. Third, dosing protocols were not standardized, complicating interpretation of potential saturation effects. In addition, the brain delineations included the ventricles, as they could not be reliably excluded on the PET/CT images in the segmentation tool (Figure 7). However, the choroid plexus, which could confound signal due to its high vascularity, was excluded. Patlak analysis also has practical limitations, requiring multiple blood samples and imaging time points, which increases patient burden compared to simpler static approaches.

Finally, the model assumes equilibrium between plasma and reversible compartment, typically reached around 24 hours post-injection (Patlak et al., 1983). In this study, earlier time points (from 17 hours onward) were included to avoid further data loss. Including data from before equilibrium may introduce upward bias in K_i estimates, as early tracer dynamics can mimic irreversible uptake before the system has stabilized.

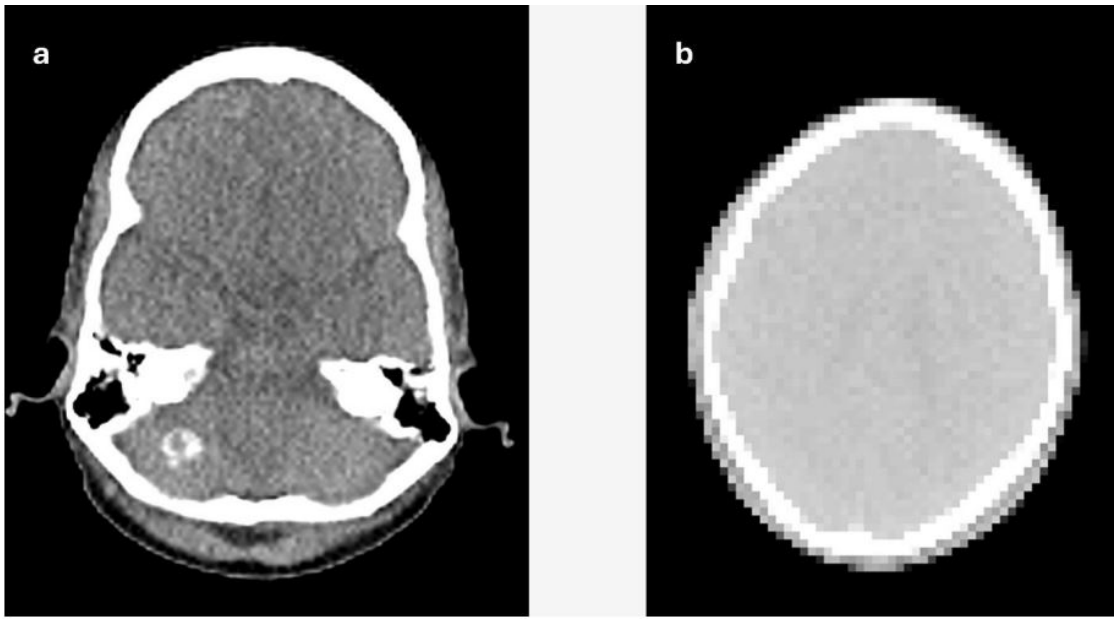

Figure 7: (a) Axial CT image from a PET/CT scan of a patient from the HER2 study, showing tracer accumulation in the peri-necrotic rim of a brain lesion. (b) PET image from a patient in the mAb 2 study, illustrating that the ventricular system is not clearly visualized with this imaging modality.

5.7 Future research

Future studies could aim to more precisely characterize tracer uptake in necrotic lesions by separately delineating the avascular, non-viable core from the peri-necrotic rim. The latter often shows increased perfusion and vascular permeability, which may contribute to non-specific antibody accumulation (Hinnen & Eskens, 2007). A key methodological improvement would be the use of high-resolution anatomical MRI scans acquired shortly before or after PET/CT. In the present study, no suitable MRI sequences were available, which meant that delineation of brain tissue and lesions had to be performed on low-dose CT. Although this allowed for basic anatomical orientation, the limited soft tissue contrast of CT reduces the accuracy of region definition. Incorporating MRI in future studies—aligned in time with PET/CT—would enable more accurate and reproducible delineation, particularly of lesion subregions such as necrotic cores and surrounding rims. However, logistical and financial considerations, such as scan availability and patient burden, should be considered.

5.8 Clinical implications

A key question in drug development is whether a therapeutic agent reaches its intended site of action. In peripheral tissues, this can sometimes be verified through biopsy, but this is usually not feasible in the brain. Blood-based biomarkers offer indirect insights but lack spatial resolution. This study demonstrates that PET imaging enables non-invasive, quantitative assessment of irreversible antibody uptake in the human brain. The K_i values provide a robust reference for non-specific uptake under intact BBB conditions, which may serve as a baseline in future therapeutic trials. If a new compound shows elevated K_i values, this could suggest target engagement. This approach may accelerate go/no-go decisions in early-phase trials, particularly in neurodegenerative diseases such as Alzheimer's disease, where conventional outcome measures require long follow-up, suffer from low test–retest reliability, and often cannot distinguish symptomatic relief from true disease modification (Mueller et al., 2006). Imaging-based markers such as K_i offer a direct and spatially specific alternative for assessing drug delivery to the brain.

6 Conclusion

In this study, we systematically quantified the background uptake of ^{89}Zr-labeled antibodies in the brain without a target, using PET/CT imaging in three patient cohorts. This background uptake is relevant because of the restrictive nature of the BBB to large molecules such as antibodies. Our results demonstrate that the K_i in the brain without a target is low but measurable, indicating limited, non-specific, irreversible uptake. In the group with a brain target, the uptake was significantly higher, which can be explained by the combination of background and specific binding to the target. The highest uptake was observed in patients with viable brain metastases, likely due to a disrupted BBB and thus increased permeability. Overall, these findings establish a quantitative reference for non-specific antibody uptake in the brain and support the use of PET-based K_i measurements as a marker to assess target engagement and drug delivery in early-phase clinical trials, especially in neurologic and neuro-oncologic indications where direct tissue access is limited.

References

Arvanitis, C. D., Ferraro, G. B., & Jain, R. K. (2020). The blood-brain barrier and blood-tumour barrier in brain tumours and metastases. *Nat Rev Cancer*, *20*(1), 26–41. 1474-1768 Journal Article Research Support, N.I.H., Extramural Research Support, Non-U.S. Gov't Research Support, U.S. Gov't, Non-P.H.S. Review England 2019/10/12 Nat Rev Cancer. 2020 Jan;20(1):26-41. doi: 10.1038/s41568-019-0205-x. Epub 2019 Oct 10.

Bachiller, S., Jiménez-Ferrer, I., Paulus, A., Yang, Y., Swanberg, M., Deierborg, T., & Boza-Serrano, A. (2018). Microglia in neurological diseases: A road map to brain-disease dependent-inflammatory response. *Front Cell Neurosci*, *12*, 488. 1662-5102 Journal Article Review Switzerland 2019/01/09 Front Cell Neurosci. 2018 Dec 18;12:488. doi: 10.3389/fncel.2018.00488. eCollection 2018.

Boellaard, R. (2009). Standards for pet image acquisition and quantitative data analysis. *J Nucl Med*, *50 Suppl 1*, 11s–20s. Boellaard, Ronald Journal Article Review United States 2009/04/22 J Nucl Med. 2009 May;50 Suppl 1:11S-20S. doi: 10.2967/jnumed.108.057182. Epub 2009 Apr 20.

Boellaard, R. (2018a). Quantitative analysis of tracer biodistributions in (sequential) whole body pet/ct studies: Biodistribution.

Boellaard, R. (2018b). Quantitative oncology molecular analysis suite: Accurate.

Bumbaca, D., Wong, A., Drake, E., Reyes, A. E., n., Lin, B. C., Stephan, J. P., Desnoyers, L., Shen, B. Q., & Dennis, M. S. (2011). Highly specific off-target binding identified and eliminated during the humanization of an antibody against fgf receptor 4. *MAbs*, *3*(4), 376–86. 1942-0870 Journal Article Research Support, Non-U.S. Gov't United States 2011/05/05 MAbs. 2011 Jul-Aug;3(4):376-86. doi: 10.4161/mabs.3.4.15786. Epub 2011 Jul 1.

Cai, D., He, Y., Yu, H., Zhang, Y., & Shi, H. (2024). Comparative benefits of ki and suv images in lesion detection during pet/ct imaging. *EJNMMI Res*, *14*(1), 98. 2191-219x Journal Article Germany 2024/10/16 EJNMMI Res. 2024 Oct 16;14(1):98. doi: 10.1186/s13550-024-01162-x.

Chen, G. Y. & Nuñez, G. (2010). Sterile inflammation: sensing and reacting to damage. *Nat Rev Immunol*, *10*(12), 826–37. 1474-1741 Journal Article Research Support, N.I.H., Extramural Review England 2010/11/23 Nat Rev Immunol. 2010 Dec;10(12):826-37. doi: 10.1038/nri2873. Epub 2010 Nov 19.

Dewhirst, M. W. & Secomb, T. W. (2017). Transport of drugs from blood vessels to tumour tissue. *Nat Rev Cancer*, *17*(12), 738–750. 1474-1768 Journal Article Research Support, N.I.H., Extramural Review England 2017/11/11 Nat Rev Cancer. 2017 Dec;17(12):738-750. doi: 10.1038/nrc.2017.93. Epub 2017 Nov 10.

Forster, J. C., Harriss-Phillips, W. M., Douglass, M. J., & Bezak, E. (2017). A review of the development of tumor vasculature and its effects on the tumor microenvironment. *Hypoxia (Auckl)*, *5*, 21–32. 2324-1128 Journal Article Review New Zealand 2017/04/27 Hypoxia (Auckl). 2017 Apr 11;5:21-32. doi: 10.2147/HP.S133231. eCollection 2017.

Heskamp, S., Raavé, R., Boerman, O., Rijpkema, M., Goncalves, V., & Denat, F. (2017). (89)zr-immuno-positron emission tomography in oncology: State-of-the-art (89)zr radiochemistry. *Bioconjug Chem*, *28*(9), 2211–2223. 1520-4812 Journal Article Research Support, Non-U.S. Gov't Review United States 2017/08/03 Bioconjug Chem. 2017 Sep 20;28(9):2211-2223. doi: 10.1021/acs.bioconjchem.7b00325. Epub 2017 Aug 24.

Hibino, S., Kawazoe, T., Kasahara, H., Itoh, S., Ishimoto, T., Sakata-Yanagimoto, M., & Taniguchi, K. (2021). Inflammation-induced tumorigenesis and metastasis. *Int J Mol Sci*, *22*(11). 1422-0067 Journal Article Review Switzerland 2021/06/03 Int J Mol Sci. 2021 May 21;22(11):5421. doi: 10.3390/ijms22115421.

Hinnen, P. & Eskens, F. A. (2007). Vascular disrupting agents in clinical development. *Br J Cancer*, *96*(8), 1159–65. 1532-1827 Journal Article Review England 2007/03/22 Br J Cancer. 2007 Apr 23;96(8):1159-65. doi: 10.1038/sj.bjc.6603694. Epub 2007 Mar 20.

Jauw, Y. W. S., Heijtel, D. F., Zijlstra, J. M., Hoekstra, O. S., de Vet, H. C. W., Vugts, D. J., Verheul, H. M., Boellaard, R., Zweegman, S., van Dongen, G., der Houven van Oordt, C. W. M., Lammertsma, A. A., & Huisman, M. C. (2018). Noise-induced variability of immuno-pet with zirconium-89-labeled antibodies: an analysis based on count-reduced clinical images. *Mol Imaging Biol*, *20*(6), 1025–1034. 1860-2002 Journal Article Research Support, Non-U.S. Gov't United States 2018/05/02 Mol Imaging Biol. 2018 Dec;20(6):1025-1034. doi: 10.1007/s11307-018-1200-4.

Jones, A. R. & Shusta, E. V. (2007). Blood-brain barrier transport of therapeutics via receptor-mediation. *Pharm Res*, *24*(9), 1759–71. 1573-904x Journal Article Research Support, N.I.H., Extramural Research Support, U.S. Gov't, Non-P.H.S. Review United States 2007/07/11 Pharm Res. 2007 Sep;24(9):1759-71. doi: 10.1007/s11095-007-9379-0. Epub 2007 Jul 10.

Keaney, J. & Campbell, M. (2015). The dynamic blood-brain barrier. *Febs j*, *282*(21), 4067–79. 1742-4658 Journal Article Review England 2015/08/19 FEBS J. 2015 Nov;282(21):4067-79. doi: 10.1111/febs.13412. Epub 2015 Sep 8.

Klemm, J. W., Van Hazel, C., & Harris, R. E. (2024). Regeneration following tissue necrosis is mediated by non-apoptotic caspase activity. *bioRxiv*. 2692-8205 Journal Article Preprint United States 2024/08/02 bioRxiv [Preprint]. 2024 Dec 20:2024.07.26.605350. doi: 10.1101/2024.07.26.605350.

Kouhi, A., Pachipulusu, V., Kapenstein, T., Hu, P., Epstein, A. L., & Khawli, L. A. (2021). Brain disposition of antibody-based therapeutics: Dogma, approaches and perspectives. *Int J Mol Sci*, *22*(12). 1422-0067 Journal Article Review Switzerland 2021/07/03 Int J Mol Sci. 2021 Jun 16;22(12):6442. doi: 10.3390/ijms22126442.

Leenders, K. L., Perani, D., Lammertsma, A. A., Heather, J. D., Buckingham, P., Healy, M. J., Gibbs, J. M., Wise, R. J., Hatazawa, J., Herold, S., & et al. (1990). Cerebral blood flow, blood volume and oxygen utilization. normal values and effect of age. *Brain*, *113 (Pt 1)*, 27–47. Leenders, K L Journal Article England 1990/02/01 Brain. 1990 Feb;113 (Pt 1):27-47. doi: 10.1093/brain/113.1.27.

Mary, P. L. & Watkins (2008). *Foundations of Clinical Research: Applications to Practice*. Financial Times Prentice Hall.

Mellman, I. & Plutner, H. (1984). Internalization and degradation of macrophage fc receptors bound to polyvalent immune complexes. *J Cell Biol*, *98*(4), 1170–7. 1540-8140 Journal Article Research Support, Non-U.S. Gov't Research Support, U.S. Gov't, P.H.S. United States 1984/04/01 J Cell Biol. 1984 Apr;98(4):1170-7. doi: 10.1083/jcb.98.4.1170.

Miedema, I. H. C., Wijngaarden, J. E., Pouw, J. E. E., Zwezerijnen, G. J. C., Sebus, H. J., Smit, E., de Langen, A. J., Bahce, I., Thiele, A., Vugts, D. J., Boellaard, R., Huisman, M. C., & Menke-van der Houven van Oordt, C. W. (2023). (89)zr-immuno-pet with immune checkpoint

inhibitors: Measuring target engagement in healthy organs. *Cancers (Basel)*, *15*(23). 2072-6694 Journal Article Switzerland 2023/12/09 Cancers (Basel). 2023 Nov 23;15(23):5546. doi: 10.3390/cancers15235546.

Mueller, S. G., Schuff, N., & Weiner, M. W. (2006). Evaluation of treatment effects in alzheimer's and other neurodegenerative diseases by mri and mrs. *NMR Biomed*, *19*(6), 655–68. Mueller, S G Journal Article Research Support, N.I.H., Extramural England 2006/09/21 NMR Biomed. 2006 Oct;19(6):655-68. doi: 10.1002/nbm.1062.

Pardridge, W. M. (2016a). Csf, blood-brain barrier, and brain drug delivery. *Expert Opin Drug Deliv*, *13*(7), 963–75. 1744-7593 Journal Article Review England 2016/03/30 Expert Opin Drug Deliv. 2016 Jul;13(7):963-75. doi: 10.1517/17425247.2016.1171315. Epub 2016 Apr 11.

Pardridge, W. M. (2016b). Re-engineering therapeutic antibodies for alzheimer's disease as blood-brain barrier penetrating bi-specific antibodies. *Expert Opin Biol Ther*, *16*(12), 1455–1468. 1744-7682 Journal Article Review England 2016/08/31 Expert Opin Biol Ther. 2016 Dec;16(12):1455-1468. doi: 10.1080/14712598.2016.1230195. Epub 2016 Sep 7.

Patlak, C. S., Blasberg, R. G., & Fenstermacher, J. D. (1983). Graphical evaluation of blood-to-brain transfer constants from multiple-time uptake data. *J Cereb Blood Flow Metab*, *3*(1), 1–7. Patlak, C S Journal Article United States 1983/03/01 J Cereb Blood Flow Metab. 1983 Mar;3(1):1-7. doi: 10.1038/jcbfm.1983.1.

Pereslete, A. M., Hughes, M. E., Martin, A. R., Files, J., Nguyen, K., Buckley, L., Patel, A., Moore, A., Winer, E. P., Dillon, D., Li, T., Tolaney, S. M., Lin, N. U., & Sammons, S. L. (2025). Analysis of her2 expression changes from breast primary to brain metastases and the impact of her2-low expression on overall survival. *Neuro Oncol*, *27*(1), 184–194. 1523-5866 Journal Article England 2024/08/31 Neuro Oncol. 2025 Jan 12;27(1):184-194. doi: 10.1093/neuonc/noae163.

Pommranz, C. M., Elmoujarkach, E. A., Lan, W., Cabello, J., Linder, P. M., Vo, H. P., Mannheim, J. G., Santangelo, A., Conti, M., la Fougère, C., Rafecas, M., & Schmidt, F. P. (2025). A digital twin of the biograph vision quadra long axial field of view pet/ct: Monte carlo simulation and image reconstruction framework. *EJNMMI Phys*, *12*(1), 31. 2197-7364 Journal Article Germany 2025/03/31 21:17 EJNMMI Phys. 2025 Mar 31;12(1):31. doi: 10.1186/s40658-025-00738-3.

Pyzik, M., Sand, K. M. K., Hubbard, J. J., Andersen, J. T., Sandlie, I., & Blumberg, R. S. (2019). The neonatal fc receptor (fcrn): A misnomer? *Front Immunol*, *10*, 1540. 1664-3224 Journal Article Research Support, N.I.H., Extramural Research Support, Non-U.S. Gov't Review Switzerland 2019/07/30 Front Immunol. 2019 Jul 10;10:1540. doi: 10.3389/fimmu.2019.01540. eCollection 2019.

RStudio Team (2025). Rstudio: Integrated development environment for r. Computer program.

Sprowls, S. A., Arsiwala, T. A., Bumgarner, J. R., Shah, N., Lateef, S. S., Kielkowski, B. N., & Lockman, P. R. (2019). Improving cns delivery to brain metastases by blood-tumor barrier disruption. *Trends Cancer*, *5*(8), 495–505. 2405-8025 Journal Article Research Support, N.I.H., Extramural Review United States 2019/08/20 Trends Cancer. 2019 Aug;5(8):495-505. doi: 10.1016/j.trecan.2019.06.003. Epub 2019 Jul 20.

Tolar, M., Abushakra, S., Hey, J. A., Porsteinsson, A., & Sabbagh, M. (2020). Aducanumab, gantenerumab, ban2401, and alz-801-the first wave of amyloid-targeting drugs for alzheimer's

disease with potential for near term approval. *Alzheimers Res Ther*, *12*(1), 95. 1758-9193 Journal Article Research Support, N.I.H., Extramural Research Support, Non-U.S. Gov't Review England 2020/08/14 Alzheimers Res Ther. 2020 Aug 12;12(1):95. doi: 10.1186/s13195-020-00663-w.

Uhlen, M., Oksvold, P., Fagerberg, L., Lundberg, E., Jonasson, K., Forsberg, M., Zwahlen, M., Kampf, C., Wester, K., Hober, S., Wernerus, H., Björling, L., & Ponten, F. (2010). Towards a knowledge-based human protein atlas. *Nat Biotechnol*, *28*(12), 1248–50. 1546-1696 Letter Research Support, Non-U.S. Gov't United States 2010/12/09 Nat Biotechnol. 2010 Dec;28(12):1248-50. doi: 10.1038/nbt1210-1248.

Wang, S. (2025). Balancing microglial density and activation in central nervous system development and disease. *Current Issues in Molecular Biology*, *5*(344).

Watakabe, T., Toya, R., Saito, T., Matsuyama, T., Shiraishi, S., Kai, Y., Shimohigashi, Y., & Oya, N. (2020). High spatial resolution digital positron emission tomography images with dedicated source-to-background algorithm for radiotherapy planning. *Anticancer Res*, *40*(5), 2567–2572. 1791-7530 Journal Article Greece 2020/05/06 Anticancer Res. 2020 May;40(5):2567-2572. doi: 10.21873/anticanres.14227.

Wijngaarden, J. E., Huisman, M. C., Jauw, Y. W. S., van Dongen, G., Greuter, H., Schuit, R. C., Cleveland, M., Gootjes, E. C., Vugts, D. J., Menke-van der Houven van Oordt, C. W., & Boellaard, R. (2023). Validation of simplified uptake measures against dynamic patlak k(i) for quantification of lesional (89)zr-immuno-pet antibody uptake. *Eur J Nucl Med Mol Imaging*, *50*(7), 1897–1905. 1619-7089 Journal Article Germany 2023/02/24 Eur J Nucl Med Mol Imaging. 2023 Jun;50(7):1897-1905. doi: 10.1007/s00259-023-06151-1. Epub 2023 Feb 23.

Wijngaarden, J. E., Huisman, M. C., Pouw, J. E. E., Menke-van der Houven van Oordt, C. W., Jauw, Y. W. S., & Boellaard, R. (2022). Optimal imaging time points considering accuracy and precision of patlak linearization for (89)zr-immuno-pet: a simulation study. *EJNMMI Res*, *12*(1), 54. 2191-219x Journal Article Germany 2022/09/07 EJNMMI Res. 2022 Sep 5;12(1):54. doi: 10.1186/s13550-022-00927-6.

7 Supplementary

7.1 Supplementary, Tables

Overview of $\mathbf{R}^2$ and $\mathbf{K}_\mathrm{i}$ values per patient and injection (Mass dose) across all studies. If $\mathbf{K}_\mathrm{i}$ was negative, the percentage decrease is shown in parentheses. The last column ("Result") indicates whether the data point was included in the analysis, based on the criteria mentioned in the Methods.

Table 4: mAb 1

Patient	**Mass dose**	$\mathbf{R}^2$	$\mathbf{K}_\mathrm{i}$	**Result**
1	1	1	5.16×10^{-6}	Accepted
1	2	0.775	-3.28×10^{-5} ($-14.4\,\%$)	Declined
2	1	1	2.76×10^{-5}	Accepted
2	2	0.793	4.30×10^{-5}	Declined
3	1	1	2.62×10^{-5}	Accepted
3	2	0.998	1.10×10^{-4}	Accepted
4	1	0.702	-1.93×10^{-5} ($-7.4\,\%$)	Declined
4	2	0.902	3.38×10^{-5}	Accepted
5	1	1	2.13×10^{-5}	Accepted
5	2	0.221	1.12×10^{-6} ($-0.8\,\%$)	Declined
6	1	0.931	3.61×10^{-5}	Accepted
6	2	0.525	-1.16×10^{-5} ($-15.7\,\%$)	Declined
8	1	0.999	1.91×10^{-5}	Accepted
8	2	1	2.93×10^{-6} ($-1.3\,\%$)	Accepted
10	1	0.851	2.46×10^{-5} ($-9.9\,\%$)	Declined
10	2	0.012	-4.25×10^{-7} ($-3.8\,\%$)	Declined

Table 5: mAb 2

Patient	**Mass dose**	$\mathbf{R}^2$	$\mathbf{K}_\mathrm{i}$	**Result**
32	1	1	2.59×10^{-5}	Accepted
32	2	1	-2.75×10^{-6} ($-0.4\,\%$)	Accepted
35	1	1	3.95×10^{-5}	Accepted
35	2	0.950	5.38×10^{-5} ($-1.2\,\%$)	Accepted
36	1	1	5.27×10^{-5}	Accepted
36	2	0.025	1.66×10^{-6} ($-8.9\,\%$)	Declined
37	1	0.999	4.03×10^{-5}	Accepted
37	2	0.933	2.49×10^{-5}	Accepted

Table 6: HER2 - no metastases

Patient	**Mass dose**	$\mathbf{R}^2$	$\mathbf{K_i}$	**Result**
3	1	0.911	1.40×10^{-5}	Accepted
4	1	0.425	5.73×10^{-6} $(-2.4\,\%)$	Declined
5	1	0.284	9.66×10^{-6} $(-11.3\,\%)$	Declined
6	1	0.0005	-2.74×10^{-7} $(-9.9\,\%)$	Declined
8	1	0.590	1.88×10^{-5} $(-3.9\,\%)$	Declined

Table 7: HER2 metastases

Patient	**Mass dose**	$\mathbf{R}^2$	$\mathbf{K_i}$	**Result**
4	L01	0.991	5.21×10^{-4}	Accepted
8	L01	0.840	6.28×10^{-4}	Declined
8	L02	0.838	6.27×10^{-4}	Declined
8	L03	0.951	1.81×10^{-3}	Accepted
8	L04	0.920	1.78×10^{-3}	Accepted
8	L05	0.842	8.97×10^{-4}	Declined

7.2 Supplementary Figure 1, study with mAb 1

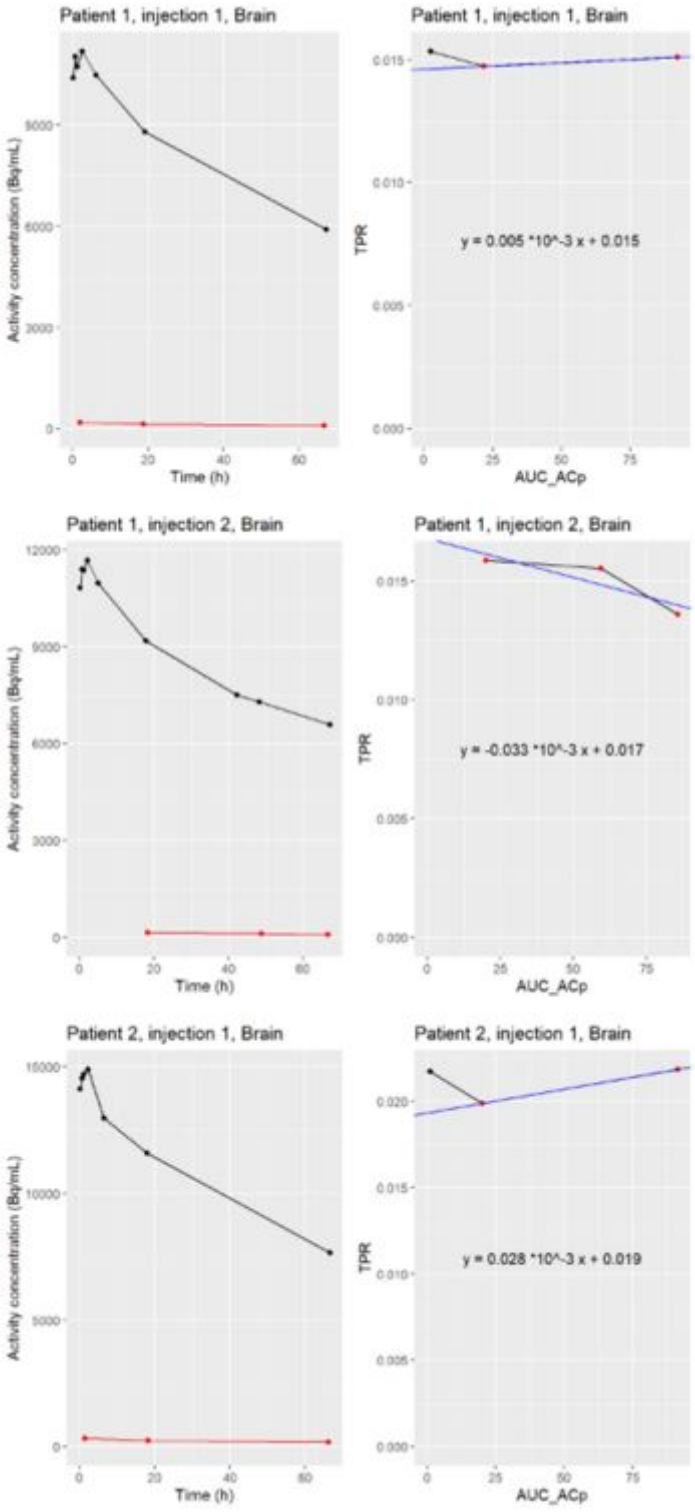

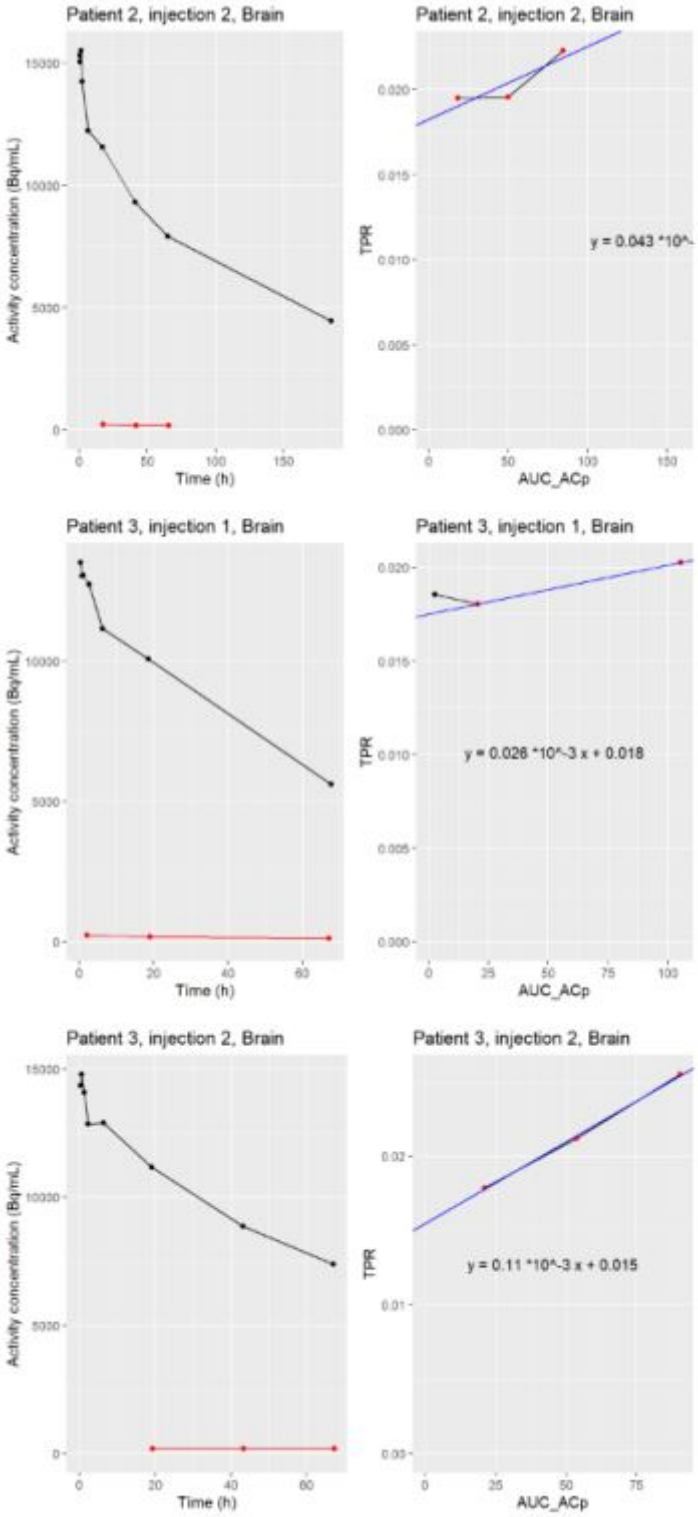
Patient 2, injection 2, Brain
Activity concentration (Bq/mL)
Time (h)
Patient 2, injection 2, Brain
TPR
AUC_ACp
Patient 3, injection 1, Brain
Activity concentration (Bq/mL)
Time (h)
Patient 3, injection 1, Brain
y = 0.026 *10^-3 x + 0.018
TPR
AUC_ACp
Patient 3, injection 2, Brain
Activity concentration (Bq/mL)
Time (h)
Patient 3, injection 2, Brain
y = 0.11 *10^-3 x + 0.015
TPR
AUC_ACp

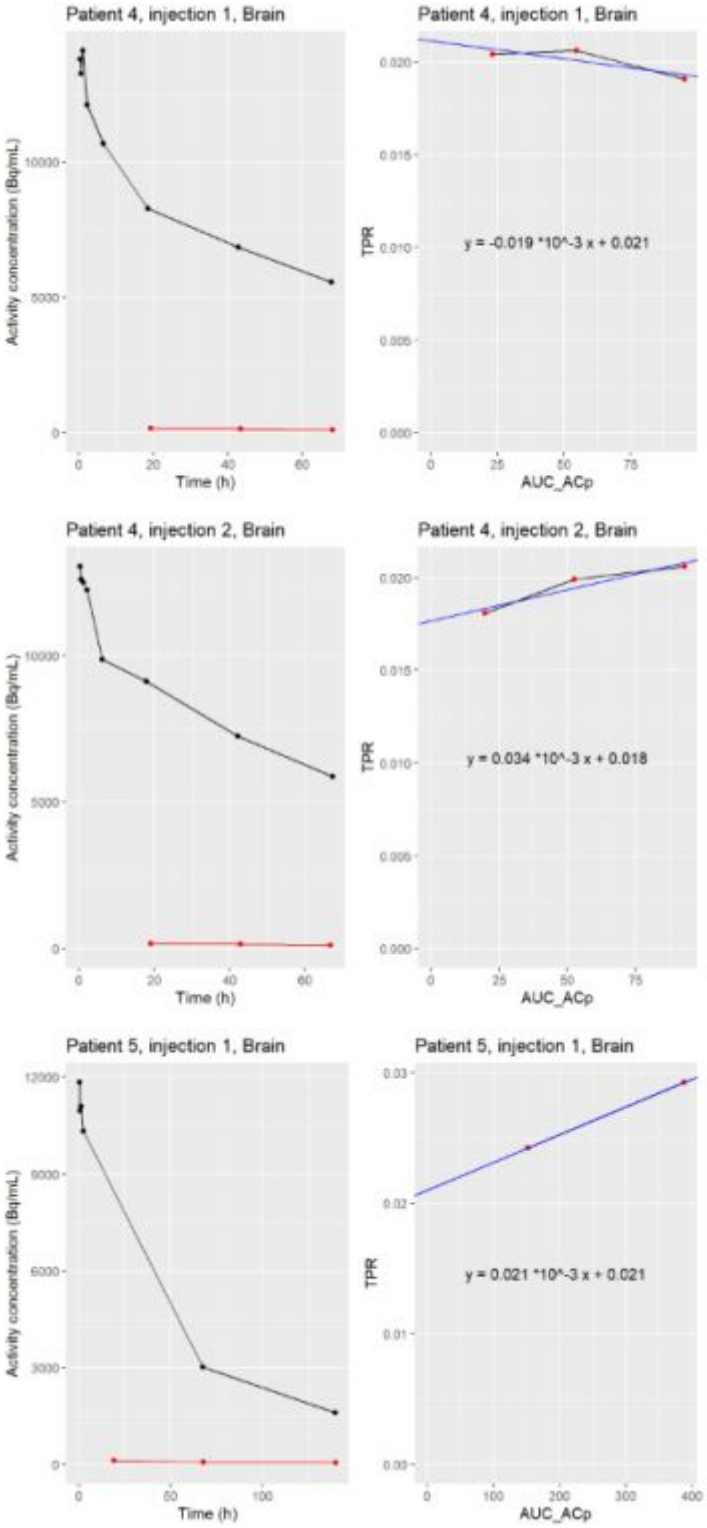
Patient 4, injection 1, Brain
Activity concentration (Bq/mL)
Time (h)
Patient 4, injection 1, Brain
TPR
y = -0.019 *10^-3 x + 0.021
AUC_ACp
Patient 4, injection 2, Brain
Activity concentration (Bq/mL)
Time (h)
Patient 4, injection 2, Brain
TPR
y = 0.034 *10^-3 x + 0.018
AUC_ACp
Patient 5, injection 1, Brain
Activity concentration (Bq/mL)
Time (h)
Patient 5, injection 1, Brain
TPR
y = 0.021 *10^-3 x + 0.021
AUC_ACp

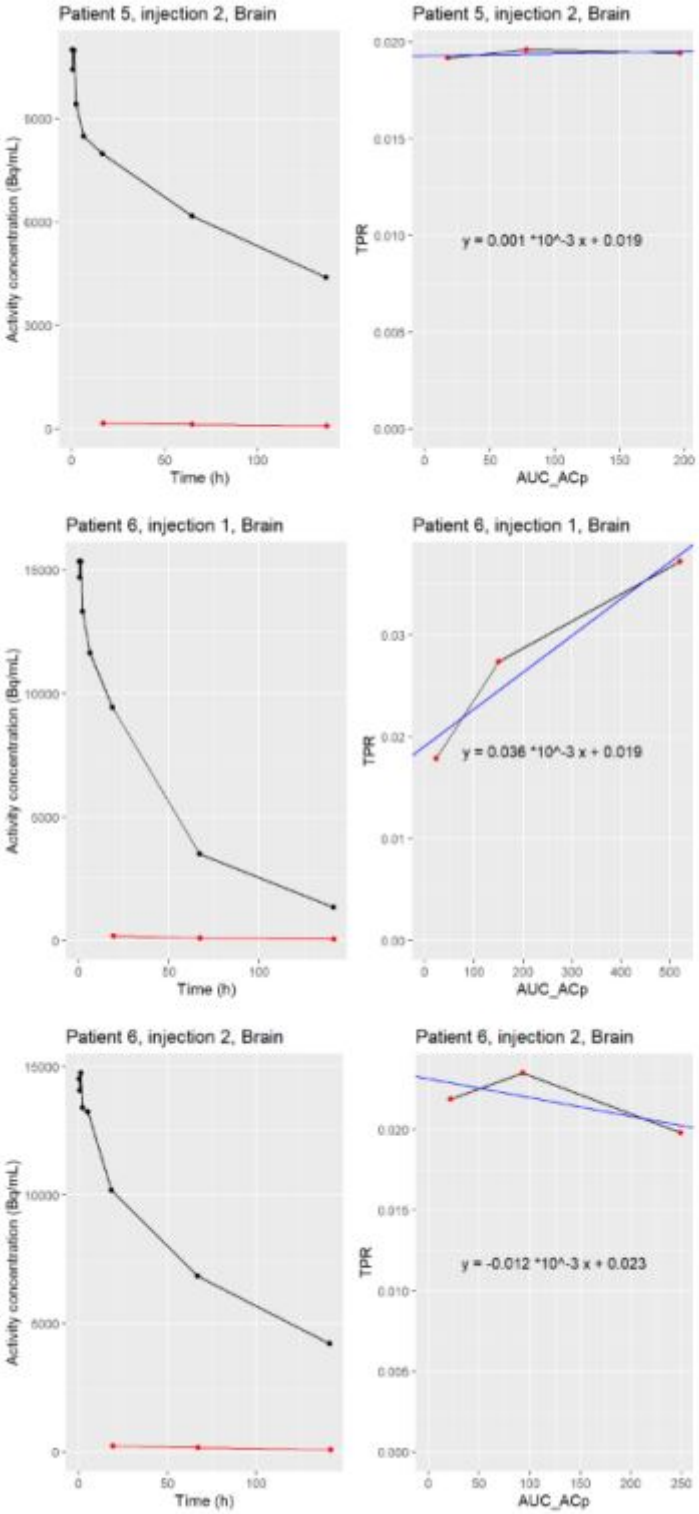
Patient 5, injection 2, Brain
Activity concentration (Bq/mL)
Time (h)
Patient 5, injection 2, Brain
TPR
y = 0.001 *10^-3 x + 0.019
AUC_ACp
Patient 6, injection 1, Brain
Activity concentration (Bq/mL)
Time (h)
Patient 6, injection 1, Brain
TPR
y = 0.036 *10^-3 x + 0.019
AUC_ACp
Patient 6, injection 2, Brain
Activity concentration (Bq/mL)
Time (h)
Patient 6, injection 2, Brain
TPR
y = -0.012 *10^-3 x + 0.023
AUC_ACp

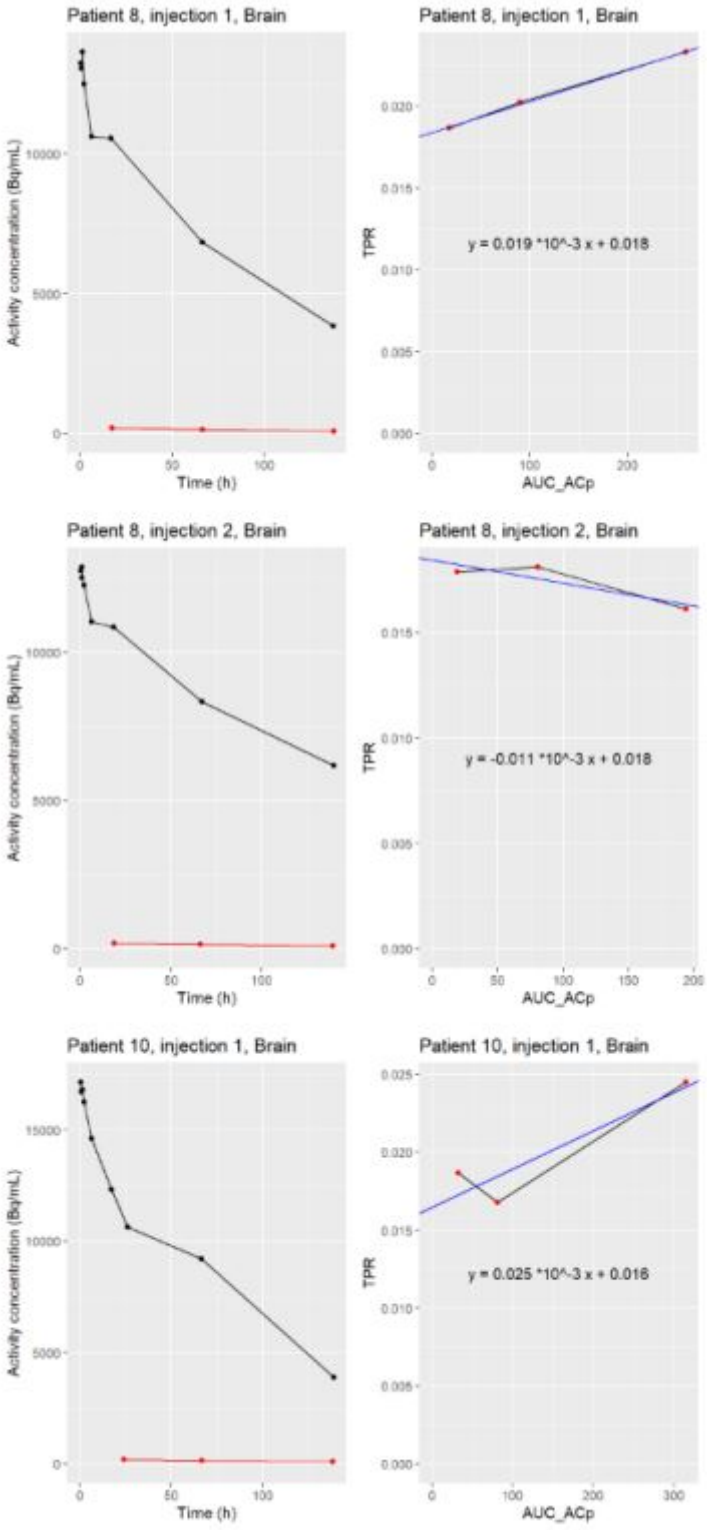
Patient 8, injection 1, Brain
Activity concentration (Bq/mL)
Time (h)
Patient 8, injection 1, Brain
TPR
y = 0.019 *10^-3 x + 0.018
AUC_ACp
Patient 8, injection 2, Brain
Activity concentration (Bq/mL)
Time (h)
Patient 8, injection 2, Brain
TPR
y = -0.011 *10^-3 x + 0.018
AUC_ACp
Patient 10, injection 1, Brain
Activity concentration (Bq/mL)
Time (h)
Patient 10, injection 1, Brain
TPR
y = 0.025 *10^-3 x + 0.016
AUC_ACp

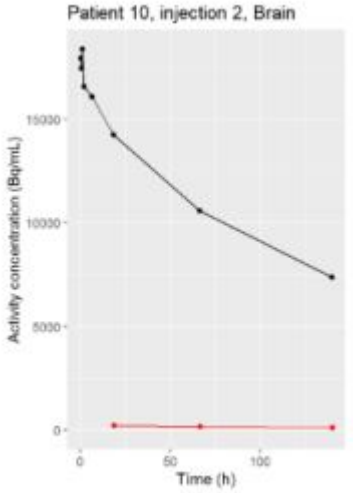
Patient 10, injection 2, Brain
Activity concentration (Bq/mL)
15000
10000
5000
0
0
50
100
Time (h)

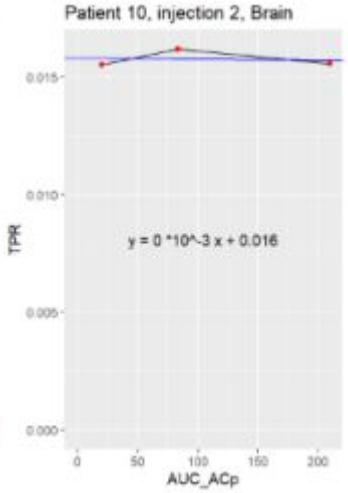
Patient 10, injection 2, Brain
TPR
0.015
0.010
0.005
0.000
y = 0 *10^-3 x + 0.016
0
50
100
150
200
AUC_ACp

7.3 Supplementary Figure 2, study with mAb 2

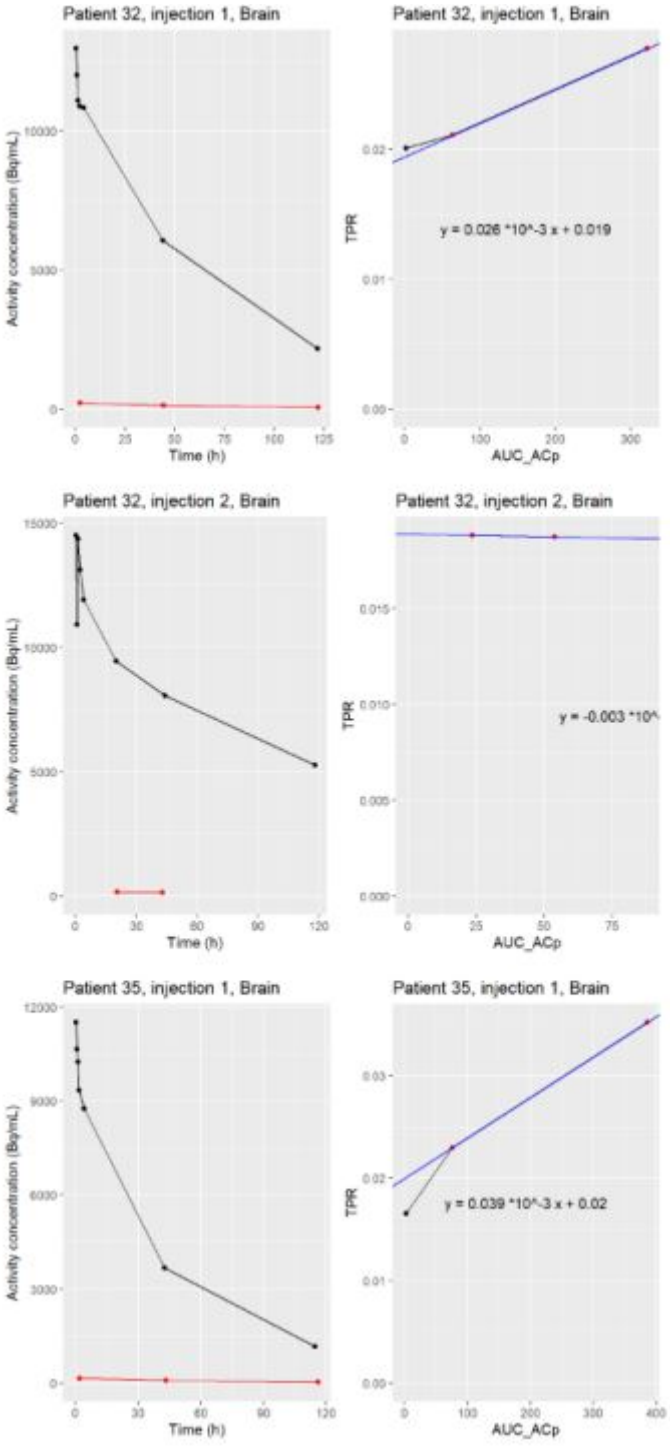

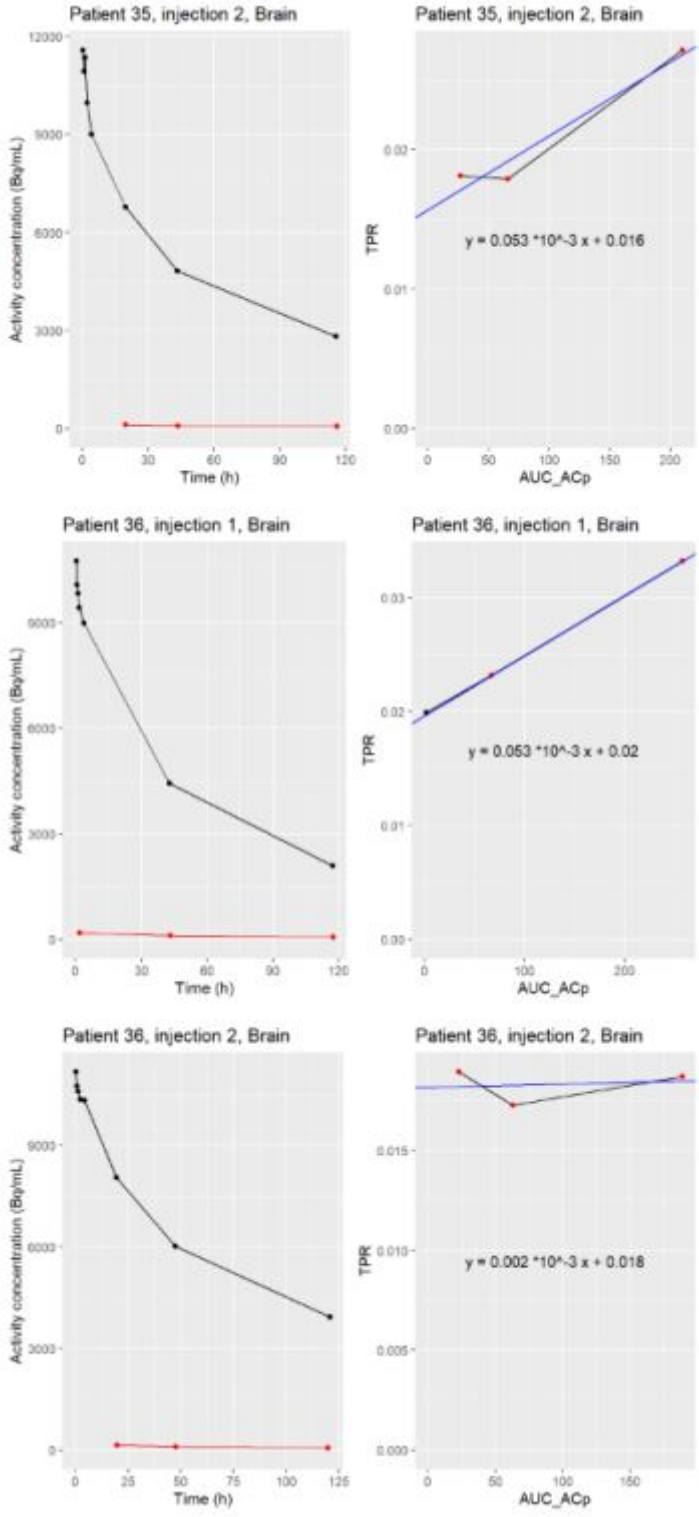
Patient 35, injection 2, Brain
Activity concentration (Bq/mL)
Time (h)
Patient 35, injection 2, Brain
TPR
y = 0.053 *10^-3 x + 0.016
AUC_ACp
Patient 36, injection 1, Brain
Activity concentration (Bq/mL)
Time (h)
Patient 36, injection 1, Brain
TPR
y = 0.053 *10^-3 x + 0.02
AUC_ACp
Patient 36, injection 2, Brain
Activity concentration (Bq/mL)
Time (h)
Patient 36, injection 2, Brain
TPR
y = 0.002 *10^-3 x + 0.018
AUC_ACp

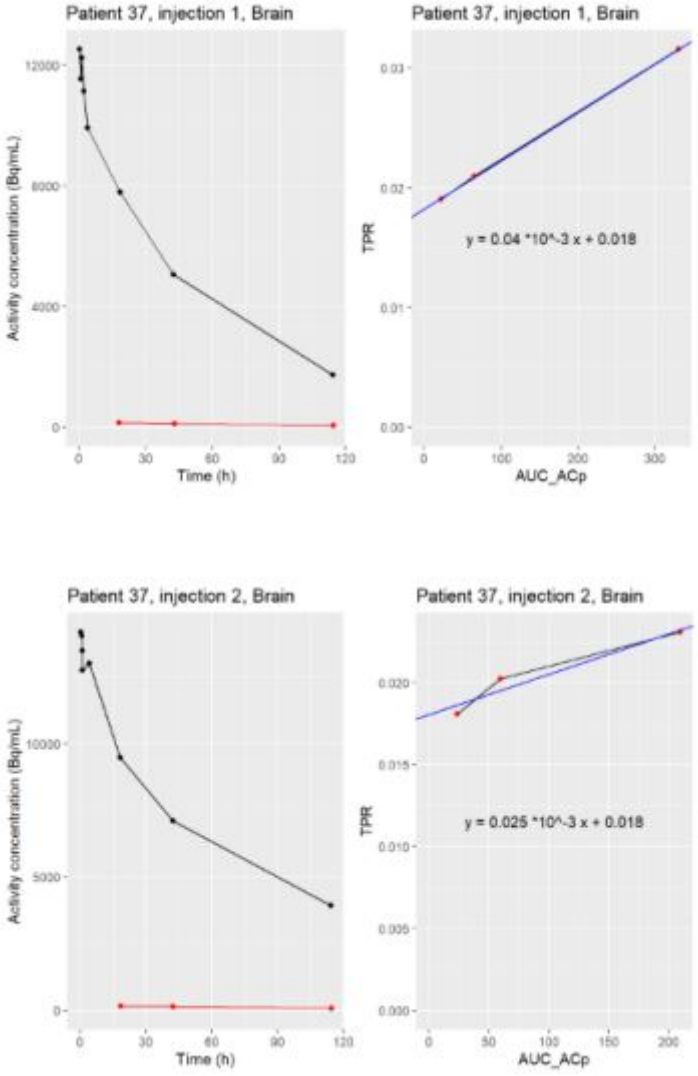
Patient 37, injection 1, Brain
Activity concentration (Bq/mL)
Time (h)
Patient 37, injection 1, Brain
TPR
y = 0.04 *10^-3 x + 0.018
AUC_ACp
Patient 37, injection 2, Brain
Activity concentration (Bq/mL)
Time (h)
Patient 37, injection 2, Brain
TPR
y = 0.025 *10^-3 x + 0.018
AUC_ACp

7.4 Supplementary Figure 3, HER2 study no metastases

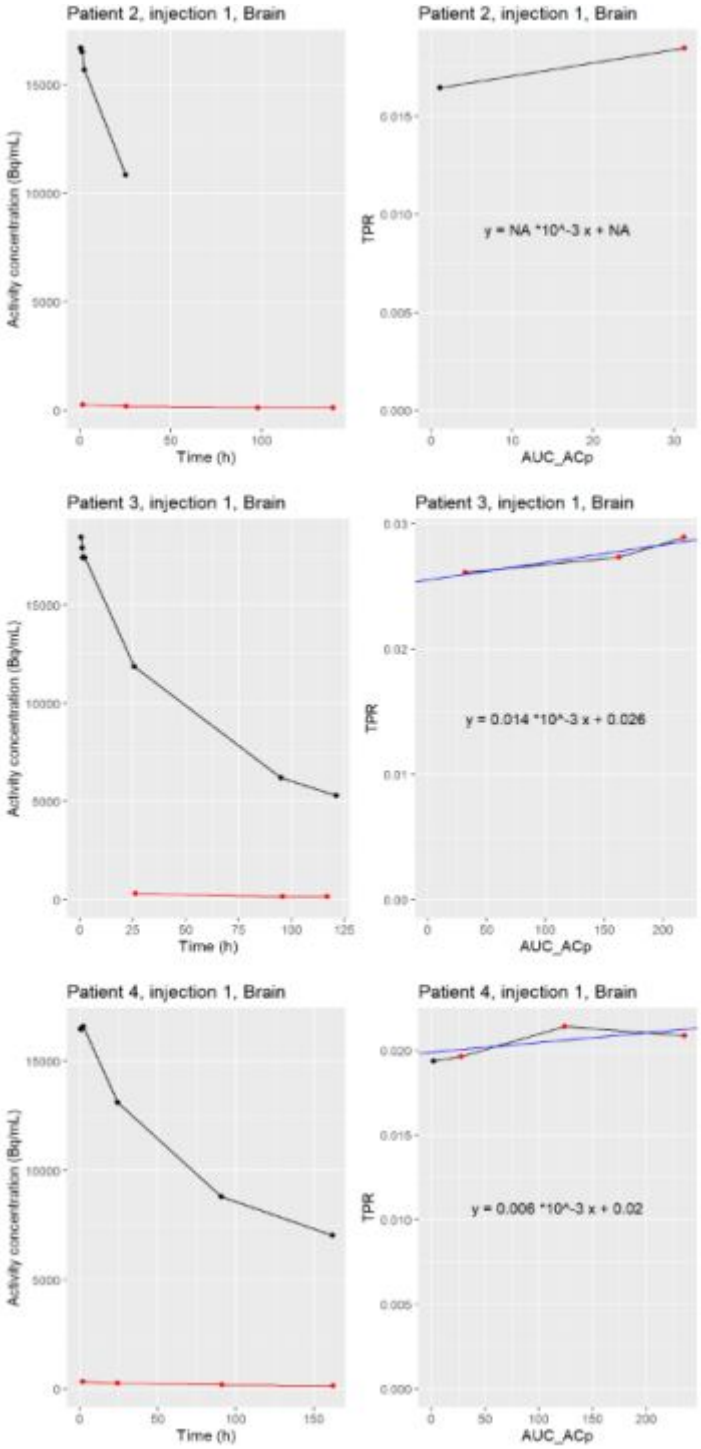

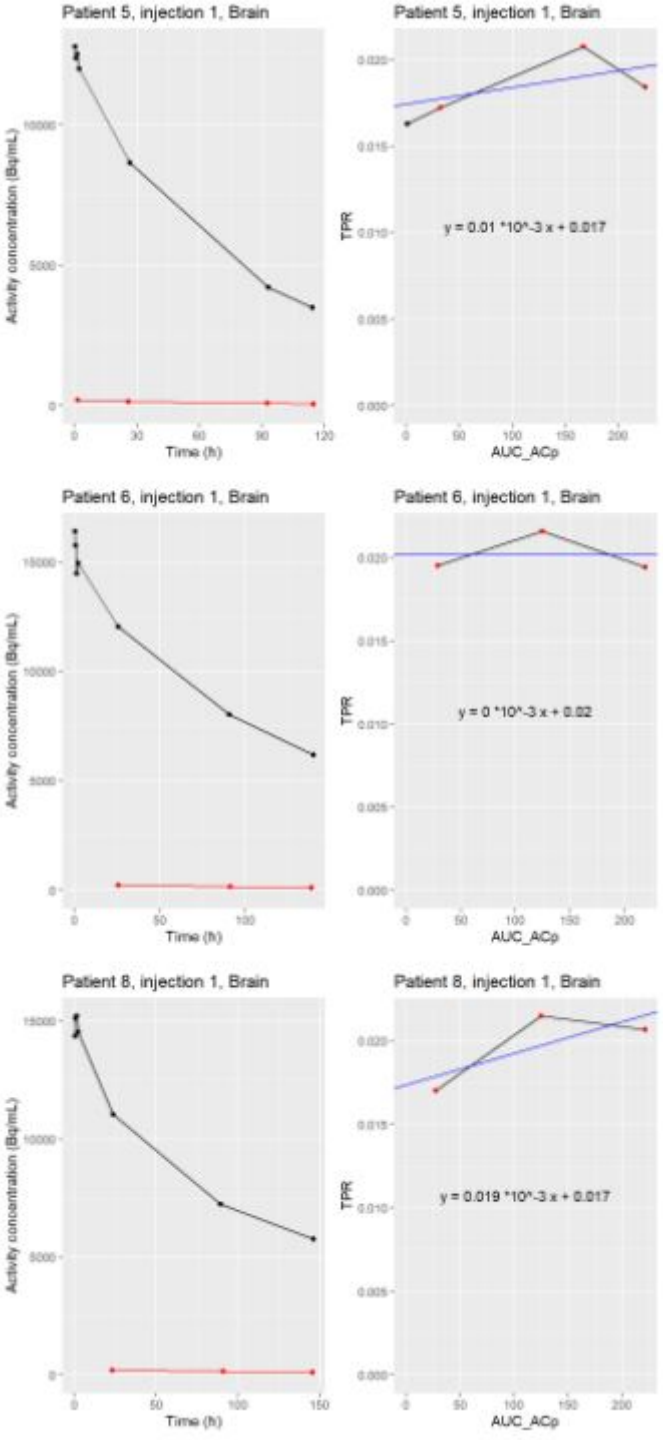
Patient 5, injection 1, Brain
Activity concentration (Bq/mL)
Time (h)
Patient 5, injection 1, Brain
TPR
y = 0.01 *10^-3 x + 0.017
AUC_ACp
Patient 6, injection 1, Brain
Activity concentration (Bq/mL)
Time (h)
Patient 6, injection 1, Brain
TPR
y = 0 *10^-3 x + 0.02
AUC_ACp
Patient 8, injection 1, Brain
Activity concentration (Bq/mL)
Time (h)
Patient 8, injection 1, Brain
TPR
y = 0.019 *10^-3 x + 0.017
AUC_ACp

7.5 Supplementary Figure 4, HER2 study metastases

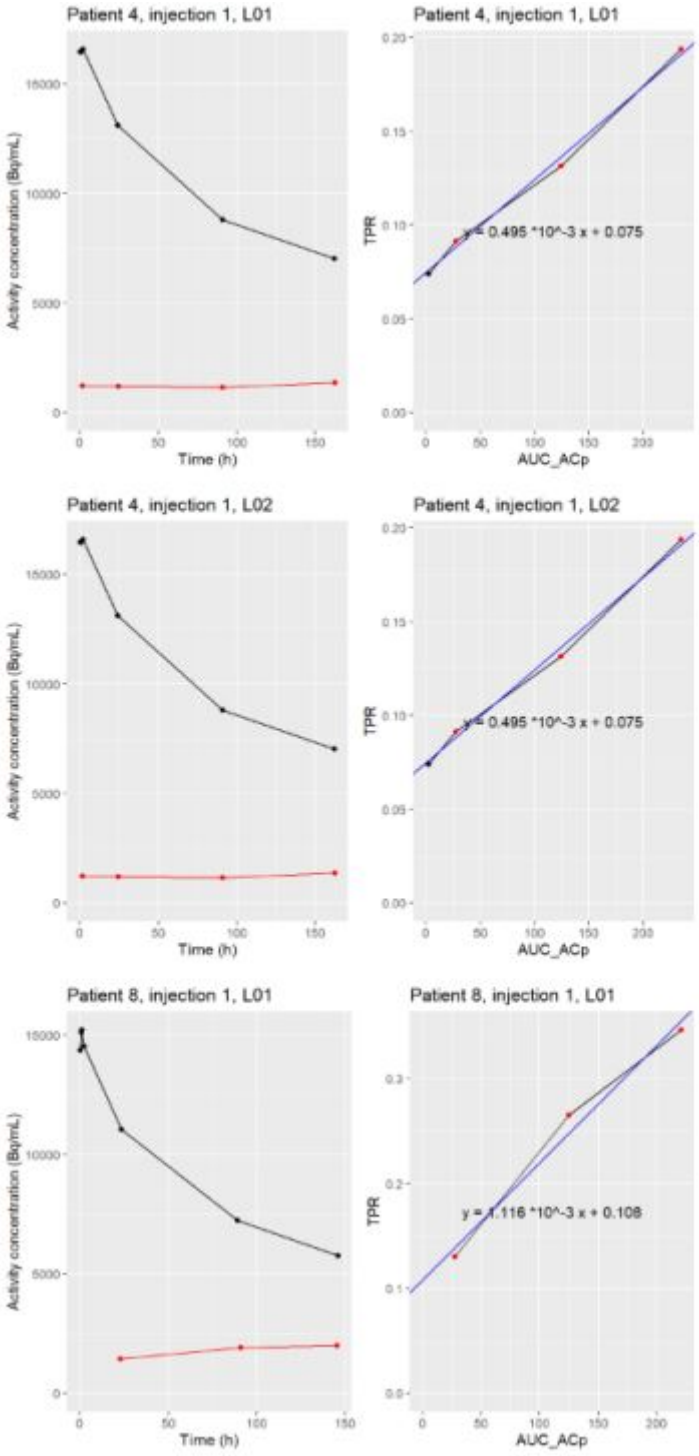

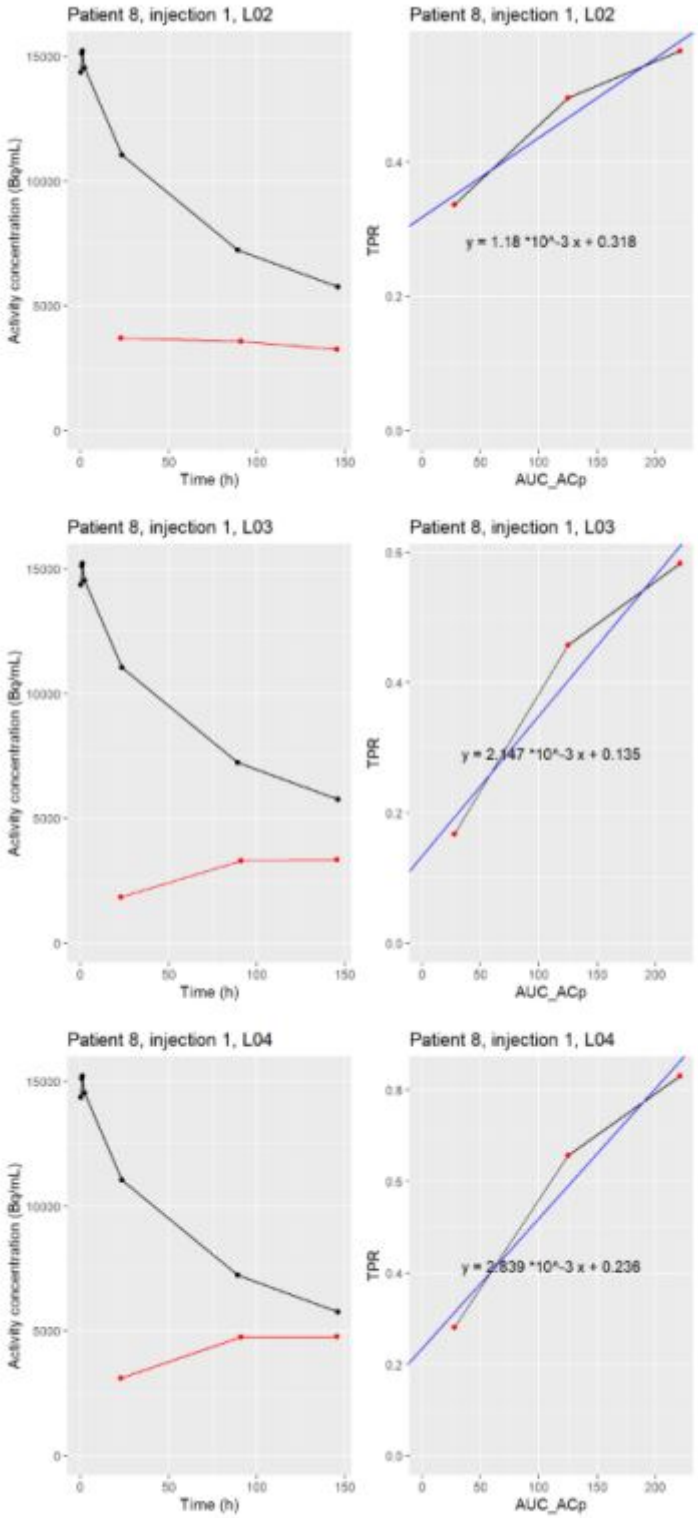
Patient 8, injection 1, L02
Activity concentration (Bq/mL)
Time (h)
Patient 8, injection 1, L02
TPR
y = 1.18 *10^-3 x + 0.318
AUC_ACp
Patient 8, injection 1, L03
Activity concentration (Bq/mL)
Time (h)
Patient 8, injection 1, L03
TPR
y = 2.147 *10^-3 x + 0.135
AUC_ACp
Patient 8, injection 1, L04
Activity concentration (Bq/mL)
Time (h)
Patient 8, injection 1, L04
TPR
y = 2.839 *10^-3 x + 0.236
AUC_ACp

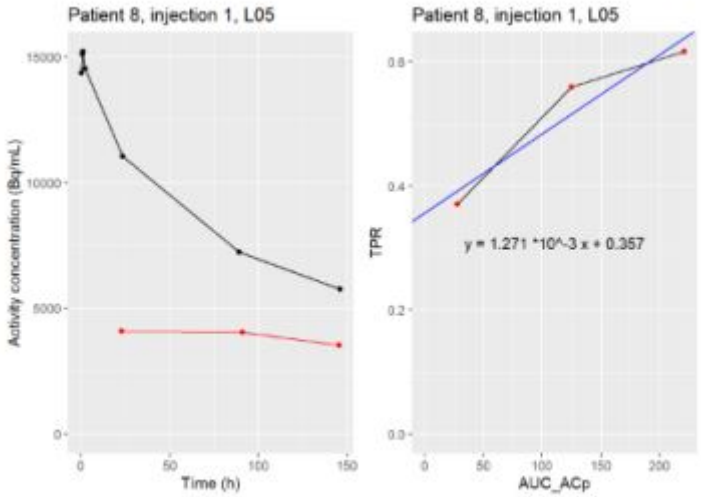
Patient 8, injection 1, L05
Activity concentration (Bq/mL)
15000
10000
5000
0
0
50
100
150
Time (h)
Patient 8, injection 1, L05
TPR
0.8
0.4
0.2
0.0
y = 1.271 *10^-3 x + 0.357
0
50
100
150
200
AUC_ACp